

to appear in the March 2000 issue of The Astronomical Journal

## Synthetic Spectra and Color-Temperature Relations of M Giants

M. L. Houdashelt,<sup>1</sup> R. A. Bell

Department of Astronomy, University of Maryland, College Park, MD 20742-2421

A. V. Sweigart

Code 681, NASA/Goddard Space Flight Center, Greenbelt, MD 20771

and

R. F. Wing

Department of Astronomy, Ohio State University, Columbus, OH 43210

### ABSTRACT

As part of a project to model the integrated spectra and colors of elliptical galaxies through evolutionary synthesis, we have refined our synthetic spectrum calculations of M giants. After critically assessing three effective temperature scales for M giants, we adopted the relation of Dyck et al. (1996) for our models. Using empirical spectra of field M giants as a guide, we then calculated MARCS stellar atmosphere models and SSG synthetic spectra of these cool stars, adjusting the band absorption oscillator strengths of the TiO bands to better reproduce the observational data. The resulting synthetic spectra are found to be in very good agreement with the K-band spectra of stars of the appropriate spectral type taken from Kleinmann & Hall (1986) as well. Spectral types estimated from the strengths of the TiO bands and the depth of the bandhead of CO near  $2.3 \mu\text{m}$  quantitatively confirm that the synthetic spectra are good representations of those of field M giants. The broad-band colors of the models match the field relations of K and early-M giants very well; for late-M giants, differences between the field-star and synthetic colors are probably caused by the omission of spectral lines of VO and H<sub>2</sub>O in the spectrum synthesis calculations. Here, we present four grids of K-band bolometric corrections and colors – Johnson U–V and B–V; Cousins V–R and

---

<sup>1</sup>Current address: Department of Physics & Astronomy, Johns Hopkins University, 3400 North Charles Street, Baltimore, MD 21218

V–I; Johnson-Glass V–K, J–K and H–K; and CIT/CTIO V–K, J–K, H–K and CO – for models having  $3000 \text{ K} \leq T_{\text{eff}} \leq 4000 \text{ K}$  and  $-0.5 \leq \log g \leq 1.5$ . These grids, which have  $[\text{Fe}/\text{H}] = +0.25, 0.0, -0.5$  and  $-1.0$ , extend and supplement the color-temperature relations of hotter stars presented in a companion paper.

*Subject headings:* stars: fundamental parameters — stars: late-type — stars: atmospheres — stars: evolution — infrared: stars

## 1. Introduction

M giants are important contributors to the integrated light of many stellar aggregates, such as early-type galaxies and galactic bulges, even though they generally comprise a very small fraction of the stellar mass of these systems. In fact, recent integrated light models of the Galactic bulge of the Milky Way (Houdashelt 1995) indicate that M giants contribute over half of the K-band flux there and thus also dictate the strength of spectral features such as the  $2.3 \mu\text{m}$  CO band. However, the relative importance of these cool stars in integrated light is quite dependent upon the wavelength region under consideration and the other stellar populations present. For example, at optical wavelengths, where the Galactic-bulge M giants are much fainter than they are in the near-infrared, these stars produce only about 10–20% of the bulge’s continuous flux but are entirely responsible for the broad absorption bands of TiO seen in this part of its spectral energy distribution. Consequently, population models of galaxies should strive to include realistic representations of M giants.

Unfortunately, M stars have proven especially difficult to model accurately because they are so cool and thus have a wealth of molecules in their stellar atmospheres. This means that a variety of phenomena which can be ignored in the modelling of hotter stars are important in the atmospheric structure of M stars. The most critical of these are the molecular opacities, which depend not only on the accuracy of the (sometimes nonexistent) laboratory data but also on the way in which the opacities are calculated and represented in the models. Simple mean opacities, opacity distribution functions and opacity sampling have each been used in the modelling of cool star atmospheres. For example, plane-parallel models of M giants have been calculated by Brett (1990) using straight mean opacities and by Jørgensen (1994) using opacity sampling.

Other factors influencing cool star models include sphericity effects and variability. In spherical models, an additional parameter is introduced – the extension of the atmosphere,  $d$ . It is defined by the relation,  $d = r/R - 1$ , where  $R$  is the stellar radius, typically defined to be the radius at which the Rosseland optical depth is equal to unity, and  $r$  is the radius at

which the Rosseland optical depth has a value of  $10^{-5}$ . Static, spherical models of M giants have been constructed by Bessell et al. (1989a), Scholz & Tsuji (1984), Scholz (1985) and Plez et al. (1992). All but the latter used straight mean opacities in their models; Plez et al. (1992) incorporated more recent opacity data and used opacity sampling. Dynamic, spherical models, representing Mira variables, have been studied by Bessell et al. (1989b) and Alvarez & Plez (1998).

Extension and sphericity are generally important for two reasons. First, if  $\log g$  varies significantly between the base of the stellar atmosphere and its outer layers, it may be necessary to include the radial dependence of gravity explicitly in the stellar atmosphere model. Second, extension results in a higher photon escape probability, and the corresponding dilution of the stellar flux produces a cooling of the outer layers of the atmosphere. Due to the temperature sensitivity of molecule formation, this cooling in turn enhances the formation of certain molecules and thus their partial pressures. In fact, extension can be so important in cool stars that Scholz & Wehrse (1982) and Scholz (1985) have suggested a 3-dimensional classification scheme for M giants in which extension serves as the third parameter (in addition to  $T_{\text{eff}}$  and  $\log g$ ); they propose that the extension of an M giant can be estimated observationally from the depths of specific TiO bands at a given effective temperature and surface gravity. However, Plez et al. (1992) has found that a good representation of the opacities is more important than sphericity effects for models having  $\log g \gtrsim 0.0$  and masses of order  $1 M_{\odot}$  or more. Thus, sphericity and variability significantly affect only the coolest of M giant models.

We have recently begun an evolutionary synthesis program to produce synthetic spectra of early-type galaxies. The foundations of this work are stellar atmosphere models and synthetic spectra calculated with updated versions of the MARCS (Gustafsson et al. 1975, Bell et al. 1976) and SSG (Bell & Gustafsson 1978; Gustafsson & Bell 1979; Bell & Gustafsson 1989; hereafter BG89) computer codes, respectively. However, because we employ versions of these codes which do not account for sphericity and other factors which affect the stellar atmospheres of M giants, we have exerted a considerable effort to fine-tune our models to compute more representative synthetic spectra of these cool stars and also to establish an effective temperature scale for M giants based upon recent angular diameter measurements. In a companion paper, Houdashelt et al. (2000; hereafter Paper I), we describe many of the recent improvements in these codes and present new color-temperature relations for stars as cool as spectral type K5.

In the present paper, we discuss our improved models of M giants and compare the resulting synthetic spectra and colors to observational data. In Section 2, we briefly describe the MARCS/SSG models and calculations, examine the possible shortcomings of using

these models to represent M giants and present our strategy for testing and refining the synthetic spectrum calculations to compensate for these shortcomings. We compare three effective temperature scales for cool stars in Section 3 and determine which best represents the field M giants. Section 4 discusses our treatment of TiO absorption in the synthetic spectra and compares our results to observed spectra of field M giants. We also show the good agreement between the computed and observed CO band strengths and compare the broad-band colors measured from the synthetic spectra to photometry of field stars. Section 5 summarizes the major conclusions of this work.

## 2. Basic Details of the M Giant Models

The models of M giants presented in this paper have been constructed in exactly the same manner as those of the hotter stars described in Paper I. We provide here only a brief description of the MARCS model atmospheres and the SSG synthetic spectrum calculations, emphasizing those factors which are most relevant to calculating models of cool stars. We refer the reader to Paper I for further details.

### 2.1. Calculating the Model Atmospheres and Synthetic Spectra

The version of the MARCS stellar atmosphere code used to construct the model atmospheres of the M giants produces a flux-constant, chemically-homogeneous, plane-parallel model atmosphere calculated under the assumptions of hydrostatic equilibrium and LTE. It incorporates opacity distribution functions (ODFs) to represent the opacity due to atomic and molecular lines as a function of wavelength.

The SSG spectral synthesis code combines the MARCS model atmosphere and spectral line lists to compute a synthetic spectrum. The primary spectral line list which we use is the updated version of the Bell “N” list (Bell et al. 1994) described in Paper I. In addition, optional line lists for TiO and H<sub>2</sub>O can be included in the calculations. We have incorporated the TiO line list in our M giant models, and we describe it more fully below. As described later in this paper (see Section 4.2.3), both of the H<sub>2</sub>O line lists which we tested were found to be unsatisfactory, so no water lines are included in the models presented here.

The TiO spectral line list includes lines from the  $\alpha$  (C<sup>3</sup>Δ–X<sup>3</sup>Δ),  $\beta$  (c<sup>1</sup>Φ–a<sup>1</sup>Δ),  $\gamma$  (A<sup>3</sup>Φ–X<sup>3</sup>Δ),  $\gamma'$  (B<sup>3</sup>Π–X<sup>3</sup>Δ),  $\delta$  (b<sup>1</sup>Π–a<sup>1</sup>Δ),  $\phi$  (b<sup>1</sup>Π–d<sup>1</sup>Σ), and  $\epsilon$  (E<sup>3</sup>Π–X<sup>3</sup>Δ) systems. In addition to the lines of <sup>48</sup>TiO, the spectral line lists include lines of <sup>46</sup>TiO, <sup>47</sup>TiO, <sup>49</sup>TiO

and  $^{50}\text{TiO}$  as well. Wavelengths and gf values for lines in the  $\epsilon$  system were kindly provided by Plez (1996). For lines of the other systems, wavelengths were calculated using molecular constants taken from Phillips (1973), and the Hönl-London factors were obtained from formulae in Kovacs (1969). The Franck-Condon factors were taken from Bell et al. (1979) for the  $\alpha$ ,  $\gamma$ ,  $\gamma'$  and  $\phi$  systems and computed for the  $\beta$  and  $\delta$  systems using the code described by Bell et al. (1976). The initial  $f_{00}$  values for the  $\alpha$ ,  $\beta$ ,  $\gamma$  and  $\gamma'$  systems came from Hedgecock et al. (1995), while those for the  $\delta$  and  $\phi$  bands were assumed to be 0.0190 and 0.0210, respectively. Improved values were found empirically by comparing observed and synthetic spectra of field M giants as described in Section 4.1.

All of the stellar atmosphere models and synthetic spectra discussed in this paper have been constructed using solar abundance ratios for all of the elements except carbon and nitrogen. Paper I discusses the evidence indicating that stars which are more evolved than the “bump” in the red-giant-branch luminosity function have had CNO-processed material mixed into their atmospheres. Consequently, we have used  $[\text{C}/\text{Fe}] = -0.2$ ,  $[\text{N}/\text{H}] = +0.4$  and  $^{12}\text{C}/^{13}\text{C} = 14$  for our M giant models, in accordance with the abundance ratios measured in field M giants (Smith & Lambert 1990).

As in Paper I, the synthetic spectra were calculated at  $0.1 \text{ \AA}$  resolution and in two pieces, optical and infrared (IR). The optical portion of the spectrum covers wavelengths from 3000–12000  $\text{\AA}$ , and the IR section extends from 1.0–5.1  $\mu\text{m}$  (the overlap is required for calculating J-band magnitudes). In addition, the microturbulent velocity,  $\xi$ , used to calculate the synthetic spectrum of a given star was derived from its surface gravity using the field-star relation,  $\xi = 2.22 - 0.322 \log g$  (Gratton et al. 1996).

## 2.2. Possible Deficiencies in the Models

There are two possible drawbacks to using our version of MARCS model atmospheres to represent M giants. First, being plane-parallel models, they do not account for the affects of sphericity and extension. Second, the ODFs which we employ do not include the molecular opacities of  $\text{TiO}$ ,  $\text{VO}$  and  $\text{H}_2\text{O}$ , which are among the strongest opacity sources in M stars. In addition, the spectral line list used by SSG does not include lines of  $\text{VO}$ . Still, there are good reasons to believe that the models, especially those of the hotter M giants, will not be too greatly in error due to these factors.

Jørgensen (1994) has shown that the inclusion of  $\text{TiO}$  in plane-parallel model atmospheres mainly serves to heat the surface layers of the models, with the extent of the heating diminishing as  $T_{\text{eff}}$  decreases. This heating inhibits the formation of  $\text{H}_2\text{O}$ , which

thus does not become an important source of opacity until mid-to-late-M types. The main effect of H<sub>2</sub>O opacity in his models is to cause an expansion of the atmosphere in cooler stars ( $T_{\text{eff}} \lesssim 3000$  K). VO appears to have little influence on the atmospheric structure but does affect the spectra of M giants, producing a series of broad absorption bands between about 0.7 and 2.2  $\mu\text{m}$  in the spectra of giants later than spectral type M5 (Brett 1990; Plez 1998).

From a physical standpoint, the basic differences between spherical model atmospheres and their plane-parallel counterparts appear to be 1) the spherical models extend to lower gas pressures and temperatures, and 2) as extension increases, the temperature at a given optical depth decreases, while the gas pressure at a given temperature increases (see e.g., Scholz & Tsuji 1984; Scholz 1985). Scholz (1985) and Bessell et al. (1989a) have found that extension is relatively unimportant in early-type M giants but dramatically increases with decreasing effective temperature for  $T_{\text{eff}} \lesssim 3500$  K, mainly due to a substantial increase in the H<sub>2</sub>O opacity. In addition, they find that extension influences only the uppermost layers of the atmosphere, so that molecular species such as TiO, VO and H<sub>2</sub>O are affected, but CN and CO, which mostly form deeper in the atmosphere, are found to be relatively insensitive to extension. Plez et al. (1992) also find that extension affects TiO formation mainly because it forms in the upper layers of the atmosphere; extension is the greatest for their models near 3200 K due to the saturation of H<sub>2</sub>O bands.

Thus, while these factors (plane-parallel model atmospheres, missing opacity in the ODFs) are potential hindrances to successful modelling of cool giants, we expect them to have relatively minor effects on our results. Since they affect only the surface layers of the models, the continuum in our models should accurately represent the effective temperature. On the other hand, we would be surprised to find that the absorption bands of the molecules formed in the outer parts of the atmosphere matched those observed in stars of the corresponding  $T_{\text{eff}}$ . The TiO bands, which are extremely temperature-sensitive, should be the most important in this regard, since VO and H<sub>2</sub>O bands are observed in the spectra of only the coolest M giants (spectral type M5 and later) and/or those of very low gravity; the omission of the latter two molecules in the ODFs probably has a minimal influence on the stellar atmosphere models of most M giants. Thus, we have good reason to believe that we can overcome the deficiencies inherent in our ODFs and plane-parallel models by modifying our treatment of TiO.

### 2.3. How Do We Test Our Models?

Quite often, stellar models are evaluated by comparing the colors of a grid of solar-metallicity models to observed color-color or color-temperature relations of field stars. If the field star relations fall within the domain of the grid colors at a given effective temperature or color, then the models are usually considered to be satisfactory. The fact that this approach is only truly appropriate for colors which are reasonable representations of the continuum slope and are relatively insensitive to gravity is often ignored. While this may be reasonable for many of the colors of hotter stars, such effects must not be neglected when modelling M giants, since their spectra are dominated by molecular absorption bands and gravity-sensitive features. It is possible that, through a fortuitous but incorrect combination of  $\log g$ ,  $[\text{Fe}/\text{H}]$  and perhaps microturbulent velocity, a synthetic spectrum can be calculated which has the colors of a field M giant of a given effective temperature but proves to be a poor match to the finer details of its spectral energy distribution. Unfortunately, without *a priori* knowledge of the temperatures and gravities of the field stars, a better way to test the model colors is not obvious.

Given the aforementioned uncertainties in our models and in dealing with cool stars in general, we do not expect to be able to produce perfect synthetic spectra of M giants. However, we need to be able to evaluate the “quality” of our models and refine them as necessary. We have chosen to do this by comparing our synthetic spectra to observed spectra of field M giants in as much detail as possible. Ideally, this would utilize a good set of empirical spectra of stars of known  $T_{\text{eff}}$ , gravity and metallicity; to the best of our knowledge, such a set of data does not exist for M giants. Instead, we have chosen to use the “intrinsic” spectral sequence of field M giants presented by Fluks et al. (1994; hereafter FPTWWS) to test and improve our synthetic spectrum calculations. However, to use this data for such a purpose, we must first assign effective temperatures and surface gravities to the stars represented by their spectral sequence.

In the MK spectral classification system, temperature classes of M giants are based primarily upon the strengths of the TiO bands (see Keenan & McNeil 1976). While this allows an MK spectral type to be assigned to any spectrum containing TiO bands, it also makes the classification of these cool stars metallicity-dependent, since the TiO band strengths depend upon the abundances of titanium and oxygen (we adopt logarithmic abundances of 4.78 and 8.87 dex for Ti and O, respectively, on a scale where  $\text{H} = 12.0$  dex). In other words, an M2 giant with solar abundances will not have the same effective temperature as a metal-poor M2 giant or an M2 giant with non-solar Ti/Fe ratios, such as stars in the Galactic bulge (McWilliam & Rich 1994). Because the TiO bands are also sensitive to gravity (see Bessell et al. 1989a) and extension (for the coolest and lowest

gravity M stars), there may be a more complex relation between spectral type and effective temperature for M giants than for hotter stars. Nevertheless, the primary factor affecting the TiO bands is  $T_{\text{eff}}$ , and the crucial step in calculating realistic models of M giants is to reproduce the specific relationship between the depths of the TiO bands (i.e., spectral type) and effective temperature which is observed in field M giants.

Thus, the first step in our modelling is to determine the spectral type,  $T_{\text{eff}}$  relation (hereafter STT relation) which holds for the field M giants; we do this in the subsequent section of this paper. We then assign a surface gravity to each M giant using a relation between  $\log g$  and  $T_{\text{eff}}$  derived from the isochrones and stellar evolutionary tracks produced as part of our evolutionary synthesis program (see Paper I and Houdashelt et al. 2001 for details). As expected from the discussion of our cool star models, the strengths of some of the TiO bands in the initial synthetic spectra failed to match the observed spectra, and we were forced to adjust the  $f_{00}$  values of the individual TiO bands to improve the overall agreement between the empirical and synthetic spectra.

### 3. The M Giant Temperature Scale

As discussed in Paper I, the most direct way to determine the effective temperature of a star is through measurement of its angular diameter,  $\phi$ , and its apparent bolometric flux,  $f_{\text{bol}}$ . These parameters can be related to effective temperature through the relation,

$$T_{\text{eff}} \propto \left( \frac{f_{\text{bol}}}{\phi^2} \right)^{0.25}. \quad (1)$$

Of course, angular diameters can be determined for only the most nearby stars and are typically measured through either lunar occultations or interferometry (e.g., speckle, intensity, Michelson). Usually, the diameter measured by these methods is that for a uniform disk, denoted  $\phi_{\text{UD}}$ , which must then be adjusted to give the limb-darkened angular diameter,  $\phi_{\text{LD}}$ , before computing the effective temperature. The limb-darkening correction is generally derived from stellar atmosphere models and is currently one of the greatest uncertainties in estimating the effective temperature, since this correction is sensitive to stellar parameters (such as  $T_{\text{eff}}$  itself) and the wavelength at which  $\phi_{\text{UD}}$  is determined.

As our main purpose in modelling M giants is to use their synthetic spectra for evolutionary synthesis of galaxies, the temperature scale that we choose must be consistent with that used in Paper I for the hotter stars, the STT relation of BG89. Since BG89 only derived effective temperatures for G and K stars, we must find a complementary relation for cooler stars. Below, we examine three different temperature relations for M0–M7

giants, each based upon angular diameter measurements – the relation given by Dyck et al. (1996; hereafter DBBR), that of Di Benedetto & Rabbia (1987; hereafter DiBR), and a temperature scale which we have derived from angular diameters measured by Mozurkewich et al. (1991) and Mozurkewich (1997), which we will hereafter collectively refer to as M97. Perrin et al. (1998) have recently estimated  $T_{\text{eff}}$  for stars even later than spectral type M7, but we have not included their results because even the most metal-rich isochrones used in our evolutionary synthesis models do not extend to such cool effective temperatures.

### 3.1. Angular Diameter Measurements

DBBR combined interferometric angular diameters of 34 stars measured with the Infrared Optical Telescope Array at  $2.2 \mu\text{m}$  and occultation diameters from Ridgway et al. (1980) to derive a relation between effective temperature and spectral type for K and M giants. Their temperatures were determined using the limb-darkening correction  $\phi_{\text{LD}} = 1.022 \phi_{\text{UD}}$ , which they derived from the stellar atmosphere models of Scholz & Takeda (1987). DBBR estimated the uncertainty in their effective temperature at a given spectral type to be approximately 95 K. They also concluded that M supergiants were systematically cooler than M giants of the same spectral type.

Di Benedetto (1993; hereafter DiB93) tabulated angular diameters of 21 stars, primarily taken from the work of DiBR and Di Benedetto & Ferluga (1990). These angular diameters were also measured at  $2.2 \mu\text{m}$  using Michelson interferometry, but the limb-darkening corrections were derived from the models of Manduca (1979); they used  $1.026 \leq \phi_{\text{LD}}/\phi_{\text{UD}} \leq 1.036$ , with an average of 1.035 for stars later than spectral type K5. DBBR noted that their uniform-disk angular diameters agreed well with those of DiBR for  $\phi_{\text{UD}} \leq 10 \text{ mas}$  but were systematically smaller (by about 10% on average) than the measurements of DiBR for larger stars.

M97 has presented uniform-disk angular diameters measured with the Mark III Interferometer at  $8000 \text{ \AA}$ . To convert these measurements to limb-darkened diameters, we used the giant-star data presented in Table 3 of Mozurkewich et al. (1991) to derive the relation,  $\phi_{\text{LD}}/\phi_{\text{UD}} = 1.078 + 0.002139 \text{ SP}$ , where SP is the M spectral class of the star (e.g., SP = 0 for an M0 star, SP = -1 for a K5 star). Paper I gives further details of the derivation of this relation.

Since BG89 were required to estimate apparent bolometric fluxes to compute effective temperatures using the infrared-flux method, they were also able to predict angular diameters of the stars they examined. Ideally, we would like to compare their predicted

diameters to those measured by the other groups. Unfortunately, the samples of DBBR and DiB93 have very little overlap with BG89: two and four stars, respectively. Thus, to examine the compatibility of the four sets of angular diameters, we compare the BG89, DBBR and DiB93 data to the measurements of M97.

The upper panels of Figure 1 show direct comparisons of these angular diameters, and the corresponding bottom panels illustrate the differences between the diameters plotted in the upper panels. The error bars shown for the BG89 angular diameters have been calculated using  $1.316 \times 10^7$  as the constant of proportionality in equation 1 (DBBR) and assuming a 4% uncertainty in  $f_{\text{bol}}$  and an uncertainty of 150 K in  $T_{\text{eff}}$  (see BG89). The other error bars have been taken directly from the respective references. In each of the panels of Figure 1, the solid line represents equality of the two sets of measurements compared there; the dotted line shows the angular diameter above which DBBR noted that their diameters differed systematically from those of DiBR. Squares, triangles and circles have been used to represent subgiants, giants and bright giants, and supergiants, respectively; filled symbols show M stars, and open symbols are G and K stars. A quantitative comparison of the  $\phi_{\text{LD}}$  measurements is given in Table 1.

Several conclusions can be drawn from Figure 1 and Table 1. First, the M97 and BG89 angular diameters are remarkably similar, a point already emphasized in Paper I. Second, while all three sets of measurements appear to be consistent for  $\phi_{\text{LD}} \leq 10.22$  mas ( $\phi_{\text{UD}} \leq 10$  mas), the M97 angular diameters are systematically greater than the others for stars larger than this. Third, the differences between the four sets of angular diameters are dominated by the M star measurements, probably because the stars with  $\phi_{\text{UD}} \geq 10$  mas tend to be M stars; in fact, the  $\phi_{\text{LD}}$  values for the G and K stars do not show systematic differences.

From the comparisons displayed in Figure 1 and summarized in Table 1, we conclude that the M97, BG89, DBBR and DiB93 angular diameters are in sufficient agreement for G and K stars to infer that effective temperatures based upon any of the other three group’s measurements would be consistent with the BG89 temperature scale for these stars, although there is certainly less scatter in the comparison with M97. However, the same conclusion cannot be drawn for the M stars, and we must evaluate the resulting STT relations individually to determine which is the most suitable for producing accurate synthetic spectra of M giants.

### 3.2. Comparing Effective Temperature Scales

DBBR and DiBR have derived very similar STT relations, even though some systematic differences exist in their angular diameter measurements for K and M giants, evidently because systematic differences in their estimates of  $f_{\text{bol}}$  largely offset the  $\phi_{\text{LD}}$  differences. To derive analogous STT relations based upon M97’s angular diameters, we have simply adopted the bolometric fluxes of DBBR and DiBR to calculate “M97” effective temperatures for the stars that each group had in common with M97.

The effects of using the various  $\phi_{\text{LD}}$  and  $f_{\text{bol}}$  measurements when calculating effective temperatures are shown in the four panels of Figure 2. The upper section of this figure shows the data reported by DBBR and DiBR in the left-hand and right-hand panels, respectively; the lower panels show the effective temperatures which result when the angular diameters of M97 are substituted for those used in the corresponding upper panels for the stars in common. As in Figure 1, triangles represent giants and circles are supergiants, but the filled symbols here are stars having  $\phi_{\text{UD}} > 10$  mas, while the open symbols are those with smaller angular diameters. The temperature errors shown in the upper panels of the figure are those quoted by DBBR and DiBR; those in the lower panels have been derived from equation 1, using  $1.316 \times 10^7$  as the constant of proportionality (DBBR) and adopting the  $\phi_{\text{UD}}$  uncertainties of M97 and the flux uncertainties of either DiBR or DBBR, as appropriate. The dotted line in each panel of Figure 2 is the STT relation quoted by Ridgway et al. (1980) and is based upon angular diameters measured from lunar occultations (not shown). The solid line is DBBR’s relation, which incorporates the Ridgway et al. (1980) measurements in addition to those plotted in the upper, left-hand panel of Figure 2. The dashed line is the STT relation of DiBR. The bold lines in the lower panels of Figure 2 are linear, least-squares fits to the data plotted in each.

From Figure 2, it is clear that the STT relations of DBBR and DiBR are very similar; the greatest difference occurs near spectral type M0. It is also true that the STT relations derived from the M97 angular diameters (the bold, solid lines in the lower panels of Figure 2) are nearly identical, regardless of whether the DBBR or DiBR bolometric fluxes are used; in fact, the resulting relations differ by less than 30 K at all spectral types from K0 to M7. Thus, for the remainder of this paper, we will no longer discuss the STT relation of DiBR or the relation derived from the DiBR bolometric fluxes using the M97 angular diameters; we will instead concentrate upon the DBBR data because it spans a broader range of spectral types.

As expected from the comparison of the M97 and DBBR angular diameter measurements, the STT relations which result from these two data sets agree nicely for the K giants but differ systematically in the M giant regime. To quantify this, we tabulate

these two  $T_{\text{eff}}$  scales and our estimates for the surface gravities of field M giants in Table 2; the calculation of these  $\log g$  values is described below. We will hereafter refer to these two STT relations as the DBBR and M97 effective temperature scales.

Note that all of the spectral types plotted in Figure 2 are those adopted by DBBR and DiB93 (which are identical to DiBR’s) and are presumably MK types, since they were generally taken from the work of Keenan and collaborators. We have confirmed this for the 29 stars observed by DBBR for which spectral types have also been measured using the 8-color photometric system of Wing (1971); Wing’s method (see Section 4.2.1) provides a quantitative way to measure spectral types of M giants on the MK system. The average difference in spectral types, in the sense Wing – DBBR, is 0.29 ( $\pm 0.42$ ) subtypes. If we use Wing’s spectral types, when available, to revise the M97 STT relation in the bottom, left-hand panel of Figure 2, it only differs from that adopted (Table 2) by +7 K at spectral type K1, –11 K at type M0 and –35 K at type M7. Thus, M97’s angular diameter measurements truly infer a different relation between  $T_{\text{eff}}$  and MK spectral type than that derived by DBBR. Since it is not clear which temperature scale is the best to use for constructing synthetic spectra of M giants, we have experimented with each and discuss the results in the following sections.

### 3.3. Testing the Effective Temperature Scales

To determine which of these two STT relations is best suited for M giant models, we have calculated model atmospheres and synthetic spectra (omitting spectral lines of TiO) for M0 through M7 giants on each  $T_{\text{eff}}$  scale given in Table 2. We assigned surface gravities to these models by consulting the solar-metallicity isochrones and evolutionary tracks used in our evolutionary synthesis program (Houdashelt et al. 2001). Specifically, we took  $\log g$  values at 100 K intervals between 3200 K and 4000 K from our 4 Gyr isochrone (3500–4000 K), 8 Gyr isochrone (3400 K), 16 Gyr isochrone (3300 K) and 0.7  $M_{\odot}$  evolutionary track (3200 K) and fit a quadratic relation to this data; this relation was used to derive the surface gravities listed in Table 2.

We compare our synthetic spectra to the “intrinsic” MK spectra of field M giants presented by FPTWWS in Figures 3 and 4. In these figures, the synthetic spectra are shown as solid lines and the FPTWWS spectra as dotted lines. The left-hand panels of the figures show the synthetic spectra constructed using the DBBR STT relation, while the right-hand panels show the analogous results when M97’s  $T_{\text{eff}}$  scale is adopted. The major uncertainty in evaluating the synthetic spectra through comparisons such as those in Figures 3 and 4 is the reliability of the MK spectral types of the “intrinsic” spectra of FPTWWS. These

authors obtained spectra of field M giants and assigned each a spectral type on the Case system using the criteria of Nassau & Velghe (1964). By scaling and averaging the spectra of all M giants within one-half subtype of an integral spectral type, FPTWWS derived what they called an “intrinsic” spectral sequence for M0–M10 giants on the Case system. To derive the analogous MK sequence, they assigned each Case “intrinsic” spectrum an MK type and then interpolated (and extrapolated) to get “intrinsic” spectra for M0–M10 giants on the MK system. The transformation between Case spectral types and MK types was derived from the relation tabulated by Blanco (1964) between Mt. Wilson and Case spectral types, assuming that Mt. Wilson types and MK types are identical (FitzGerald 1969; Mikami 1978). However, the latter assumption is questionable at early-M types (Wing 1979). In addition, Blanco’s transformation equates an M0 giant on the Case system to an M1.4 giant on the MK system, so extrapolation of FPTWWS’s observational data was required to produce their “intrinsic” MK spectra of M0 and M1 giants. For these reasons, we proceed cautiously when comparing our synthetic spectra to FPTWWS’s spectral sequence, especially at early-M spectral types, but we have nevertheless found their data to be extremely useful in guiding us toward improving our synthetic spectra of M giants and determining the effective temperatures of these stars. Unless otherwise specified, all further references to FPTWWS’s “intrinsic” spectra can be assumed to mean those on the MK system.

As discussed in Section 2.2, the continuum-forming regions of the stellar atmosphere are deep enough to be unaffected by sphericity, and we therefore expect the synthetic spectrum which has the same effective temperature as a star of a given spectral type to match the “continuum” (i.e., inter-TiO) regions of the observed spectrum of that star. We also expect the main differences between the empirical spectra and the synthetic spectra to be due to missing spectral lines in the synthetic spectra. This then implies that the synthetic spectrum of the correct  $T_{\text{eff}}$  should not have a lower flux than the corresponding “intrinsic” spectrum over any extended wavelength regime.

At spectral type M0, where the M97 and DBBR temperature scales only differ by 25 K, a 3880 K synthetic spectrum indeed proves to be a reasonable fit to these “continuum” regions in the FPTWWS spectrum of an average M0 giant. In fact, for spectral types M0–M3, the “continuum” region extending from 7300 to 7600 Å in the FPTWWS spectra is well-matched by the synthetic spectra calculated from the DBBR STT relation; for later types, this region is depressed in the FPTWWS spectra, with respect to the respective DBBR synthetic spectra, probably due to the appearance of TiO and/or VO absorption in the field stars. Figure 3 also suggests that the DBBR effective temperature for spectral type M1 is perhaps a bit too hot, but this could be due to errors in the aforementioned extrapolation of the FPTWWS spectra as well.

Alternatively, while the synthetic spectrum expected to represent a given spectral type on the M97 scale often produces a good fit to the inter-TiO regions blueward of 7000 Å, the poorer agreement at redder wavelengths makes these fits less satisfactory than the DBBR results for two reasons. First, TiO absorption is expected to affect the flux in the bluer regions of the spectrum for spectral types as early as K5, so there may not be any actual continuum points at visual wavelengths. Second, even though the M97 synthetic spectra fit the bluer pseudo-continuum, the fact that they are cooler than the corresponding DBBR models means that they have a flux deficit over much of the spectrum for  $\lambda > 7000$  Å. For these reasons, we conclude that the M97 temperature scale does not describe field M giants.

Why doesn't the M97 STT relation produce models which agree with the field M giant observations, when the agreement between the M97 and BG89 angular diameters for hotter stars is so remarkable? One could conclude that something is wrong with the M97 angular diameter measurements, implying that the BG89 temperatures are also incorrect. However, we propose instead that the temperature errors are not caused by faulty  $\phi_{UD}$  measurements but are due to incorrect estimates of the limb-darkening correction.

Note that Mozurkewich et al. (1991) and Mozurkewich (1997) measure angular diameters at 8000 Å, where the emergent flux of M stars is affected by TiO absorption (see Figures 3 and 4). However, TiO was not included in the models of Manduca (1979) which Mozurkewich et al. (1991) used to calculate limb-darkening corrections. Since TiO forms much higher in the stellar atmosphere than the layers in which the continuum is produced, the radiation at 8000 Å comes from a part of the atmosphere much closer to the surface of the star than that seen at continuum wavelengths. This means that a smaller limb-darkening correction is called for at 8000 Å in M giants than is appropriate at continuum wavelengths.

Consequently, the limb-darkened angular diameters of the Mozurkewich et al. (1991) M giants, which we subsequently used to derive the corrections for the M97 data, are too large and result in effective temperatures for these stars which are too cool (see equation 1). However, for hotter stars in which the TiO absorption at 8000 Å is negligible, the limb-darkening corrections are correct. This explains the good agreement between the M97 and BG89 angular diameters, since BG89 observed only G and K giants. Assuming that the STT relation of DBBR given in Table 2 is accurate for solar-metallicity M giants, we can force the M97 temperature scale to match DBBR's by altering the limb-darkening corrections which we applied to M97's data. In this way, the limb-darkening corrections which should be applied to uniform-disk angular diameters measured at 8000 Å can be estimated. For K giants, the equation derived previously,  $\phi_{LD}/\phi_{UD} = 1.078 + 0.002139$  SP, is appropriate; for M0–M4 giants, we suggest  $\phi_{LD}/\phi_{UD} = 1.059 - 0.03317$  SP; and for giants

later than type M5, a constant value,  $\phi_{\text{LD}}/\phi_{\text{UD}} = 0.906$ , can be used.

#### 4. The M Giant Models

Based upon the comparison discussed in the previous section, we have chosen to use the STT relation of DBBR to model M giants. The second column of Table 2 gives the effective temperature and surface gravity (in parentheses) which we assign to K and M giants of a given spectral subtype. The next step in constructing representative M giant synthetic spectra is to include TiO in the calculations, adjusting the TiO band strengths as necessary to try to match the spectra of field M giants.

As mentioned previously, we have used the “intrinsic” MK spectra of M giants published by FPTWWS to evaluate our synthetic spectra. In this process, we have concentrated upon the models of M2–M5 giants. We discount the stars cooler than this because they are probably variable, and their spectra are significantly affected by absorption bands of molecules not included in our ODFs and/or spectral line lists, notably VO and H<sub>2</sub>O. At spectral types M0 and M1, the FPTWWS spectra are more uncertain than those of later types because they are extrapolations of the observational data.

Our synthetic spectra of M2–M5 giants, calculated with the TiO line list and original TiO molecular data described in Section 2.1, are compared to the FPTWWS spectra in Figure 5, where the synthetic spectra are again represented by solid lines and the observational data by dotted lines. In this figure, we see that the strength of the  $\gamma$ -system TiO band near 7100 Å matches the observed depth quite well, but the agreement for most of the other TiO bands is much less satisfactory. This has led us to adjust the TiO data used in the calculations to attempt to produce better agreement with the observational data. These adjustments and the resulting spectra are discussed in the following section.

##### 4.1. Treatment of TiO

When performing spectral synthesis, especially for abundance analyses, it is common to determine “astrophysical” oscillator strengths (i.e., gf values) for individual spectral lines. For example, if a line of an element of known abundance is stronger or weaker in the synthetic solar spectrum than it is in the observed spectrum of the Sun, the gf value for that line is often adjusted until the appropriate line strength is achieved. We have chosen to use a similar approach to model the TiO bands in our synthetic spectra of M giants.

The band absorption oscillator strength for the 0–0 transition of each system of TiO

( $f_{00}$  in the notation of Larsson 1983) is less well-known than the Franck-Condon factors and the Hönl-London factors of the various TiO lines. Consequently, we have revised the  $f_{00}$  values of the TiO systems to reproduce the TiO band strengths seen in the FPTWWS spectra at a given effective temperature. For the redder bands of TiO, which lie at least partially outside the wavelength regime covered by the FPTWWS spectra, we have also used the spectra of Terndrup et al. (1990; hereafter TFW) and Terndrup et al. (1991) as guides in adjusting the TiO band strengths. Because many of the absorption bands seen in the spectra of M giants are made up of overlapping systems of TiO, a set of synthetic spectra were first calculated, each of which contained spectral lines from only one system of TiO. By isolating spectral features (or parts of features) which were dominated by bands from a single system of TiO, we were able to unambiguously adjust the  $f_{00}$  values of the individual systems. Simply for reference, Table 3 compares the  $f_{00}$  values which we eventually adopted to some others found in the literature. The resulting synthetic spectra of M giants are shown in Figure 6, where we compare our final spectra to the FPTWWS spectra. The agreement here is a significant improvement over that seen in Figure 5, especially for  $\lambda < 7000 \text{ \AA}$ . However, some discrepancies remain and merit further discussion.

There are large differences between the FPTWWS spectra and our synthetic spectra in the wavelength region of 7600–8500  $\text{\AA}$ , especially for the earliest M types. We suspect that this discrepancy is due to an error in the FPTWWS data, perhaps due to flux-calibration errors or miscorrections for telluric absorption, since the synthetic spectra calculated by FPTWWS showed similar systematic differences from their “intrinsic” field-star spectra. In the upper panel of Figure 7, we support this proposition by comparing our synthetic spectrum of an M2 giant (solid line) to FPTWWS’s analogous spectrum (dotted line), the spectrum of the M2 III star, HD 100783 (dashed line), observed by TFW, and the spectrum of HR 4517 (points), a field M1 giant observed by Kiehling (1987). The lower panel shows the telluric corrections applied to the observational data by FPTWWS (dotted line) and by Houdashelt (1995) to the TFW spectrum (solid line); the  $z$  band of telluric  $\text{H}_2\text{O}$  centered near 8200  $\text{\AA}$  clearly influences the region of interest. It is also clear from this figure that the general shape of the TiO absorption in this region of the synthetic spectrum is quite similar to that seen in HD 100783 and HR 4517. At other wavelengths, the spectra of FPTWWS, TFW and Kiehling are in much better accord. Note also that the disagreement between the synthetic spectra and the FPTWWS spectra near 8000  $\text{\AA}$  in Figure 6 decreases for later spectral types, possibly because the TiO absorption begins to dominate the telluric contamination.

Nevertheless, Figure 6 shows that there are other spectral regions, mostly located between the synthetic TiO bands, in which the calculations are evidently missing some source of opacity, since the synthetic spectra are brighter than the field star spectra there;

these occur near 5400, 6500, 7000 and 7500 Å. To explore the possibility that some of the missing absorption could be supplied by higher-order rotational-vibrational lines of TiO than those included in our line list, we computed synthetic spectra using the TiO line lists of Jørgensen (1994); these include all lines up to  $J=199$  with  $v'$  and  $v''$  values between 0 and 10. However, the use of Jørgensen’s line list did not produce a noticeable difference in the depths and morphology of the TiO bands in the optical region of the spectrum. The  $\alpha$  and  $\beta$  systems of the two line lists were indistinguishable in the synthetic spectra and only minor differences were apparent for the  $\gamma$  and  $\gamma'$  systems; the reddest bands of the latter two systems had bandheads which were sharper and bluer but fit the observed spectra less well when Jørgensen’s data were used. For the  $\delta$  system, on the other hand, the TiO bands computed from Jørgensen’s line list had a more similar morphology to those seen in the observational data, being very wedge-shaped, as opposed to the more U-shaped bands produced by our line list. While similar differences were apparent in the shapes of the synthetic  $\phi$ -system bands, we could not unambiguously detect these bands in any of the empirical spectra, so no determination could be made regarding which line list was more appropriate to use for this system. Finally, the bandheads of Jørgensen’s  $\epsilon$  system fall about 150 Å bluer than predicted by the corresponding TiO line list of Plez (1996), which produces a good match to the observational data. Thus, the discrepancies between our synthetic spectra and the FPTWWS field star spectra do not appear to be due to missing high-order lines of the systems of TiO included in our spectral line list.

Plez (1998) has kindly provided us with plots of the a–f system of TiO and the spectrum of VO absorption in a 3300 K model. It appears that most of the (inter-TiO region) differences between our synthetic spectra and the field star spectra, as well as some of those removed by altering the  $f_{00}$  values of the other TiO systems, could be rectified by inclusion of these two absorption systems in the SSG spectral line list. However, the missing opacity near 6500 Å does not appear to be due to either TiO or VO, and until we can test these possibilities further, we remain uncertain of the source of the missing opacity shortward of 7000 Å in our synthetic spectra. Keeping this caveat in mind, we will proceed to examine our models further through more qualitative and quantitative comparisons of spectral-type estimates, equivalent width measurements and broad-band colors of the synthetic spectra and field M giants.

## 4.2. Molecular Bands in the Synthetic Spectra

The main molecular species which influence the spectra of all M giants are TiO and CO. Other molecules, such as CN, VO and H<sub>2</sub>O, are also present in the atmospheres of

these stars, but their effects are important in a more limited subset of the M giants. CN is most prevalent in the earliest M types but even then is often contaminated by overlapping spectral features due to other molecules. Absorption bands of VO and H<sub>2</sub>O are seen only in spectral types M5 and later. In the following, we discuss the CO and TiO band strengths in our synthetic spectrum calculations and compare the results to observed trends and to empirical spectra of field M stars.

#### 4.2.1. *TiO and Spectral Classification*

As mentioned previously, the spectral types of M stars on the MK system are determined from the strengths of the TiO bands. For a given star, spectral classification involves comparing the observed spectrum of the star to similar spectra of standard stars which define the MK types, a somewhat qualitative method for determining spectral classes which is not unlike the comparisons we have made in Figure 6. While this might lead us to conclude that we have achieved our goal of reproducing the field giant relation between spectral type and effective temperature, it would be reassuring to be able to verify this through something more robust than a fit-by-eye. Thus, we have also estimated spectral types from our synthetic spectra using three quantitative measures of the TiO band strengths.

Wing (1971) has designed an 8-color photometric system for determining spectral types of late-K and M giants; we illustrate the filter passbands of this system in the upper panel of Figure 8 along with our synthetic spectrum of an M3 giant. Wing’s system uses the bluest of his filters (filter 71 in Figure 8) to measure the depth of the band of the  $\gamma$  system of TiO near 7100 Å and estimate a spectral type for the star, after correcting for the overlying CN absorption. Since this method relies on a single TiO band, it is obviously applicable only to stars for which this specific band is detectable and is not saturated; this turns out to be spectral types K4 through M6.

We have measured synthetic colors on Wing’s system and calculated spectral types for our synthetic spectra using the methodology described by MacConnell et al. (1992). However, before determining these spectral types, we had to calibrate the synthetic Wing colors to put them onto the observational system. This was done in a manner similar to that used to calibrate the near-infrared, broad-band colors presented in Paper I. First, the zero point corrections to be applied to the synthetic Wing magnitudes were determined from the differences between the observed magnitudes of Vega (MacConnell et al. 1992) and those measured from our synthetic spectrum of Vega (Paper I). After applying these zero-point corrections to the synthetic Wing magnitudes of 35 of the field stars modelled in Paper I,

photometry of these stars was used to derive linear relations between the photometric and synthetic colors. These calibration relations were then applied to the synthetic Wing colors of the M giant models before determining their spectral types.

TFW defined a number of spectral indices (pseudo-equivalent widths) which measure the strengths of TiO bands between 6000 and 8500 Å. For two of these indices, S(7890) and I(8460), Houdashelt (1995) presented relationships between the index and spectral type for field stars of spectral type M1 and later. The spectral regions used to define these two indices are shown alongside our synthetic spectrum of an M3 giant in the bottom panel of Figure 8. The S(7890) index measures the strength of an absorption trough due primarily to a  $\gamma$ -system band of TiO with respect to a single “continuum” sideband. The I(8460) index measures the strength of a bandhead of the  $\epsilon$  system of TiO with respect to a pseudo-continuum level interpolated from two adjacent spectral regions, the bluer of which is affected by TiO absorption due to bands of both the  $\gamma$  and  $\delta$  systems. We have measured these indices from the M-giant synthetic spectra shown in Figure 6 and used Houdashelt’s relations to estimate their spectral types.

In the upper panel of Figure 9, we compare the spectral types measured from our synthetic spectra using Wing’s photometric system to those implied by the effective temperatures of the models per the DBBR STT relation. The agreement is excellent, with the difference between the derived and expected spectral types being larger than 0.3 subtypes only for spectral types M0, M1 and M5. Since the agreement is good at spectral type K5, we suspect that the larger discrepancies for the M0 and M1 stars occur because the effective temperatures of the models are slightly too warm at these spectral types. In effect, this simply means that DBBR’s temperature estimate for an M1 giant is a bit too hot. Since they did not list  $T_{\text{eff}}$  for spectral type M0, such a problem would affect the temperature at this spectral type as well because we have taken a simple average of their K5 and M1 temperatures to get  $T_{\text{eff}}$  for type M0. Figure 3, which was consulted to decide which effective temperature scale to adopt, supports the notion that the  $T_{\text{eff}}$  of a field M1 giant is hotter than that which DBBR estimated but implies that the M0 temperature cannot be too far off, again with the caveat that the FPTWWS “intrinsic” spectra for spectral types M0 and M1 are extrapolations of their data and are therefore somewhat uncertain. At spectral type M5, the difference between the Wing spectral type and that inferred from the model’s  $T_{\text{eff}}$  may well be due to some of the previously-discussed model uncertainties. Judging from Figure 6, it is apparent that the “continuum” bands in our synthetic spectra, especially the region near 7500 Å which is integral in determining Wing spectral types, are brighter than observed in the FPTWWS spectra. Since the 75 and 78 filters of Wing’s system (see Figure 8) are definitely affected by VO absorption in late-M giants, it is likely that the Wing spectral types of the models cooler than about 3500 K are

later than those observed in the corresponding field giants mainly because we don’t include lines of VO in our spectral synthesis.

In the middle and lower panels of Figure 9, we compare the spectral types derived from the S(7890) and I(8460) indices to the types assigned from the effective temperatures of the models. These diagrams can be broken into two parts: early-M types (M1–M4) and late-M types (M5–M7). For the former group, the  $\gamma$ -system band of TiO with bandhead near 7600 Å, which dominates S(7890), is probably a little too weak in our models (or there is insufficient flux in the single continuum sideband), while the  $\epsilon$ -system bandhead measured by the I(8460) index appears about right. For the later types, the S(7890) index gives spectral types agreeing with the effective temperatures, but the I(8460) types appear to be too strong. Unfortunately, since both the S(7890) and I(8460) indices lie in the region of the spectrum where we suspect FPTWWS’s spectra to be in error (see Figure 7), the information which can be gleaned about these indices through comparisons of the synthetic spectra and the observational data is limited. Nevertheless, we will briefly discuss possible implications of these TiO index measurements in the synthetic spectra.

It appears that the  $\gamma$ -system band of TiO which produces most of the absorption measured by the S(7890) index may truly be too weak in our synthetic spectra. Because VO absorption would apparently have a greater affect on the pseudo-continuum region used to measure S(7890) than on the spectral region of the index itself (Plez 1998), this could be true even at later spectral types; adding spectral lines of VO to the synthetic spectra would probably weaken the S(7890) indices for models having  $T_{\text{eff}} \lesssim 3500$  K. On the other hand, making this band stronger by increasing the  $f_{00}$  value of the  $\gamma$  system would throw off the good agreement between the synthetic spectra and FPTWWS’s “intrinsic” spectra in other spectral regions; for example, the absorption band with bandhead near 7100 Å is also dominated by a  $\gamma$ -system band, as is the redder half of the band between 6500 and 7000 Å. Thus, given the uncertainties in the calibration between S(7890) and spectral type and the overall good agreement between the synthetic spectra and the empirical data, we have chosen not to “tweak” this band to produce S(7890) spectral types which agree better with those inferred by the model temperatures.

Figure 6 shows that the TiO absorption affecting the I(8460) index does appear to grow more quickly with decreasing  $T_{\text{eff}}$  in the synthetic spectra than in the corresponding FPTWWS spectra. However, the spectral region in which the I(8460) index is measured is highly composite – the sharp bandhead is due to a band of the  $\epsilon$  system of TiO, but there are overlying TiO bands from the  $\delta$  and  $\gamma$  systems as well. We again believe that adding spectral lines of VO to the synthetic spectrum calculations would largely resolve the differences between the I(8460) spectral types and the temperature-inferred types of the

M5–M7 giants.

Even with the above considerations, the differences between the spectral types estimated from the TiO bands of the synthetic spectra and those indicated by their effective temperatures are small, always less than 1.2 spectral subtypes. Thus, we conclude that the strengths of the TiO bands in our synthetic spectra are in sufficient agreement with those expected from their effective temperatures that we can be confident that the synthetic spectra which we calculate will provide a good representation of M giants in our evolutionary synthesis models.

#### 4.2.2. *CO and Spectral Classification*

One of the strongest absorption bands in cool giants is the first-overtone  $^{12}\text{CO}(2,0)$  band with bandhead near  $2.3 \mu\text{m}$ . In fact, Baldwin et al. (1973) designed an intermediate-band filter system specifically to measure the strength of this band; these filters were later refined by Cohen et al. (1978) into the set commonly used today. Baldwin et al. showed that their CO index is a good luminosity indicator in cool stars, being stronger in giants than in dwarfs of similar color; they found that the index varies with  $T_{\text{eff}}$  in giants as well, becoming stronger as  $T_{\text{eff}}$  decreases. Bell & Tripicco (1991) have attributed the gravity behavior of this feature to the lower continuous opacity in the atmospheres of cool giants with respect to those of cool dwarfs of similar effective temperature; this effect more than compensates for the lower abundance of molecules in the giant’s atmosphere.

In a series of papers, the CO index was studied in field dwarfs (Persson et al. 1977), Galactic globular and open cluster members (Cohen et al. 1978; Frogel et al. 1979; Persson et al. 1979; Cohen et al. 1980; Frogel et al. 1981; Frogel et al. 1983), Magellanic Cloud clusters (Persson et al. 1983) and globular clusters in M31 (Frogel et al. 1980). Frogel et al. (1978; hereafter FPAM) have characterized the CO indices of field dwarfs and giants as a function of color, and Frogel et al. (1975), FPAM, and Persson et al. (1980) used the CO indices of early-type galaxies and the nuclear region of M31 to infer that the (infrared) integrated light of these objects must be giant-dominated.

Because this CO band is so gravity-sensitive, it is an important stellar population diagnostic in integrated light studies, and CO is a potentially informative spectral feature when applying our evolutionary synthesis models to interpret observational data. We expect to be able to model the CO bands effectively in M giants, since CO forms deep enough in the stellar atmosphere to be relatively unaffected by extension and sphericity. In fact, Bell & Briley (1991) have shown that the behavior of the  $2.3 \mu\text{m}$  CO band with gravity and

metallicity can be modelled quite reliably in G and K stars with MARCS/SSG synthetic spectra, but we wish to verify that this condition still holds for the current models, given the improvements made to the ODFs and CO spectral line data (see Section 2.1 and Paper I) since their work.

In Figures 10 and 11, we compare our synthetic spectra of the appropriate spectral type to each of the spectra of field M giants observed by Kleinmann & Hall (1986; hereafter KH86). The agreement between the synthetic spectra and the KH86 spectra is quite good throughout the entire temperature range of M giants, even at spectral type M7, where the field stars of KH86 are variable. The  $^{13}\text{CO}$  bandheads at 2.345 and 2.365  $\mu\text{m}$  can be seen in Figures 10 and 11 as well and indicate that the  $^{12}\text{CO}/^{13}\text{CO}$  ratio varies among the KH86 M giants.

More recently, Ramírez et al. (1997; hereafter RDFSB) have developed a scheme by which the equivalent width of the 2.3  $\mu\text{m}$  CO band,  $\text{EW}(\text{CO})$ , can be used to find effective temperatures for K and M giants. They obtained spectra of field stars at low and intermediate resolutions ( $R=1380$  and  $R=4830$ ) and measured  $\text{EW}(\text{CO})$  for these stars, using slightly different continuum band definitions at each resolution. After converting spectral type to effective temperature, RDFSB found a linear relationship between  $\text{EW}(\text{CO})$  and  $T_{\text{eff}}$ . Because there did not appear to be any systematic differences between their  $R=1380$  and  $R=4830$  measurements, they combined all of their data to derive this relation.

We have convolved and rebinned our synthetic spectra of K and M giants to match each resolution and dispersion of RDFSB and have measured  $\text{EW}(\text{CO})$  using their continuum and CO band definitions. We have also measured  $\text{EW}(\text{CO})$  from the KH86 spectra using both the  $R=4830$  and  $R=1380$  continuum definitions. In Figure 12, we compare our measurements of  $\text{EW}(\text{CO})$  as a function of spectral type to those of RDFSB. In this diagram, we have taken the spectral types of the RDFSB stars from SIMBAD, so they sometimes differ slightly from those adopted by RDFSB; for our synthetic spectra, we assume the spectral types indicated from the STT relation of DBBR. Since our  $\text{EW}(\text{CO})$  measurements *do* show a resolution dependence, we plot the  $R=4830$  results in the upper panels of Figure 12 and the  $R=1380$  results in the lower panels. The left-hand side of this diagram shows the relations between  $\text{EW}(\text{CO})$  and spectral type at each resolution; here, the data from RDFSB is shown as open circles, our KH86 measurements are asterisks, the solid lines connect the  $\text{EW}(\text{CO})$  values measured from our synthetic spectra, and the dotted lines are linear, least-squares fits to the RDFSB data. On the right-hand side of the figure, the spectral types of the synthetic spectra, derived from the dotted relations shown in the left-hand panels, are compared to the spectral types inferred by DBBR’s STT relation.

Some general conclusions can be drawn from Figure 12. As expected from the

comparisons shown in Figures 10 and 11, the  $\text{EW}(\text{CO})$  measurements of the synthetic spectra are in good agreement with those of the KH86 spectra, with the CO absorption perhaps a bit stronger in the synthetic spectra than in the KH86 spectra for the K giants. At  $R=4830$ , the synthetic spectrum CO widths and RDFSBS’s CO widths agree well for the M giants, with the CO again a bit stronger in the K-giant synthetic spectra than in the observational data. At  $R=1380$ , the situation is reversed from that observed at  $R=4830$ ; the synthetic spectra and the RDFSBS spectra produce very similar  $\text{EW}(\text{CO})$  for the K giants, but in this case, the CO bands of the synthetic spectra of the M giants (and the KH86 spectra) appear weaker than in the RDFSBS spectra. Detailed comparisons of the RDFSBS spectra and our synthetic spectra indicate that these discrepancies are not due to differences in the strengths of the CO bands but instead are caused by differences in the slope of the continuum just blueward of the  $^{12}\text{CO}$  bandhead.

Overall then, given the scatter in the  $\text{EW}(\text{CO})$  measurements of RDFSBS, and keeping in mind that a linear fit between  $\text{EW}(\text{CO})$  and spectral type does not appear to apply over the entire range of K and M spectral types, we conclude that the spectral types estimated for the synthetic spectra from their CO equivalent widths are in agreement with those based upon their effective temperatures, especially at  $R=4830$ . Since K and M giants dominate the near-infrared light of most stellar populations, Figures 10, 11 and 12 also show that our treatment of the CO absorption in these cool stars will produce a realistic representation of the CO bands in our evolutionary synthesis models.

#### 4.2.3. $\text{H}_2\text{O}$

SSG has the option of including a spectral line list for water in the spectrum synthesis calculations, but we have opted not to include  $\text{H}_2\text{O}$  absorption in the models presented here. This omission is based upon synthetic spectra calculated using the water line lists of Brett (1991) and Schryber et al. (1995). Brett’s line list is derived from the laboratory data of Ludwig et al. (1973) using the method described by Plez et al. (1992), while the list of Schryber et al. (1995) is theoretical.

We first calculated models including spectral lines of  $\text{H}_2\text{O}$  using the line list of Schryber et al. (1995), but the water absorption seen in the resulting synthetic spectra differed substantially from expectations based upon observational data. The  $\text{H}_2\text{O}$  lines depressed the flux much more evenly throughout the infrared than is observed and did not show the familiar strong bands which occur, for example, between the H and K atmospheric windows. In addition, the agreement between the observed and calculated CO bands was substantially worsened in the coolest models which included these  $\text{H}_2\text{O}$  lines. While the use

of Brett’s data produced spectra in which the water vapor bands were more discrete, the bands which overlapped the CO absorption again were sufficiently strong to spoil the nice agreement between the synthetic and the empirical spectra seen in Figures 10 and 11.

To date, we have not been able to determine whether the behavior of the H<sub>2</sub>O absorption in the models is due to problems with the stellar atmosphere models, which possibly predict an overabundance of water, or the spectral line lists, which may have oscillator strengths which are too large. It is possible that, to reproduce the spectrum of H<sub>2</sub>O seen in real stars, the water absorption in our synthetic spectra would require a treatment similar to that which we have used for TiO. Unfortunately, observational data from the Infrared Space Observatory, for example, is not yet available to allow us to verify the need for such an empirical calibration. Nevertheless, since water absorption is not detectable in the spectra of M giants until spectral type M5 or later (Bessell et al. 1989a), the evolutionary synthesis models which we construct should not be significantly affected by the omission of water lines in our synthetic spectra.

### 4.3. Broad-Band Colors and Bolometric Corrections of K0–M7 Field Giants

We have measured broad-band colors from our spectral-type sequence of K and M giant synthetic spectra – Johnson U–V and B–V; Cousins V–R and V–I; Johnson-Glass V–K, J–K and H–K; and CIT/CTIO V–K, J–K, H–K and CO – using the filter transmission profiles described in Paper I. We have also computed CIT/CTIO K-band bolometric corrections (BCs) for these models, assuming  $M_{K,\odot} = +3.31$  and  $BC_{K,\odot} = +1.41$ . We present these colors and BCs in Table 4; all of the colors have been transformed to the observational systems using the color calibrations derived in Paper I. Because these color calibrations are all very linear, we feel comfortable extrapolating them into the regime of M giant synthetic colors, even though the sample of field stars used to determine the calibration relations did not include any stars cooler than spectral type K5. However, as in Paper I, we caution the reader that the U–V and H–K colors have greater uncertainties than the other colors; the U–V colors are sensitive to missing opacity in the ultraviolet region of the synthetic spectra, and the H–K color calibrations are not well-determined (see Paper I).

In Figures 13 and 14, we compare our color vs.  $T_{\text{eff}}$  and color vs. spectral type relations to those observed for field M giants. We have extended these comparisons into the K giant regime to illustrate the general agreement between the models and field relations for hotter stars. In each of these figures, our models are represented by open circles, and the M giant photometry presented by FPTWWS is shown as small crosses. We have also measured colors directly from the “intrinsic” MK spectra of FPTWWS which we used to calibrate

the TiO bands, and these colors are shown as filled triangles in Figure 13. The field relations appear as solid and dotted lines; their sources are described below and in the figure captions. The filled squares seen in the upper panels of Figure 14 will be described as those specific panels are discussed.

Figure 13 shows the optical color comparisons, and the agreement between the models and the observational data is generally quite good. The color-temperature relations shown in the left-hand panels of Figure 13 have been taken from Gratton et al. (1996; dotted lines) and Bessell (1998; solid lines); the latter were derived from the data of Bessell et al. (1998). The field-star color, spectral type relations shown as solid lines in the right-hand panels come from Lee (1970) for B–V and from Thé et al. (1990) for V–R and V–I, after first converting the latter’s Case spectral types to MK types using the transformation given by FPTWWS; the dotted relation in the V–I, spectral type panel is taken from Bessell & Brett (1988; hereafter BB88).

The calibrated, optical, synthetic colors and the colors measured from the FPTWWS spectra agree for the early-M giants and then begin to diverge for the later types. The B–V colors of the FPTWWS spectra show a bit of random scatter, and the model B–V colors may be a bit too red ( $\sim 0.04$  mag) for early-M giants, but the synthetic colors fall well within the range of the FPTWWS photometry. However, if we assume that any differences between the magnitudes measured from the FPTWWS spectra and those measured from the models are due to “errors” in the model magnitudes, then a close inspection of the synthetic magnitudes shows that the B–V colors of the models are about right only because these “errors” in B and V largely offset one another.

In the V–R and V–I vs.  $T_{\text{eff}}$  panels of Figure 13, the model colors, the field relations and the colors measured from FPTWWS’s spectra are essentially identical for spectral types earlier than type M4. At cooler temperatures, the models and the FPTWWS spectrum colors differentiate mainly because missing opacity in the synthetic spectra makes their V-band magnitudes too bright. For the coolest stars, it is likely that variability, errors in the effective temperature determinations and possibly small number statistics make the field giant color-temperature relations and the FPTWWS “intrinsic” spectra less certain as well.

The analogous V–R and V–I vs. spectral type comparisons are a little more confusing. First, the model colors and the FPTWWS spectrum colors again agree to about spectral type M4 in both V–R and V–I, so we are doing a good job of reproducing the FPTWWS spectra with our synthetic spectrum calculations. Second, FPTWWS’s R-band photometry is evidently not on the Cousins system, since their V–R colors overlie neither the colors measured from their spectra nor the model colors. Finally, the field star relations don’t

appear to be well-determined – the Thé et al. (1990) and BB88 field relations differ by  $\sim 0.2$  mag in V–I at a given spectral type, and the two relations approximately bracket both the models and the colors measured from the FPTWWS spectra. This disagreement merits some further discussion.

BB88 derived the field relation (dotted line) shown in the lower, right-hand panel of Figure 13 from a combination of V–I photometry taken from Cousins (1980) and spectral types taken from the Michigan Spectral Survey (Houk & Cowley 1975; Houk 1978; Houk 1982). The relation of Thé et al. (1990), the solid line, comes from their own photometry and Case spectral types derived from their objective-prism spectra; we used FPTWWS’s transformation from Case to MK spectral types to get the relation plotted, so it is perhaps a bit more uncertain than BB88’s relation. Of course, if this transformation is incorrect, then the MK spectral types of the “intrinsic” spectra of FPTWWS are also in error, and our treatment of the TiO bands in the synthetic spectra is wrong as well. Still, let us suppose that the uncertainties in the transformation between Case and MK spectral types allow a shift to earlier spectral types of the Thé et al. (1990) relation, the models and the FPTWWS spectrum colors to make them agree with BB88’s field-giant relation. Even then, FPTWWS’s photometry (crosses) would not be similarly affected. FPTWWS took the MK spectral types of these stars from the Bright Star Catalogue (Hoffleit & Jaschek 1982), so to make these points lie along BB88’s relation requires systematic errors in FPTWWS’s photometry; this is at least conceivable, given that their V–R colors appear to be systematically too blue in the middle, right-hand panel of Figure 13.

On the other hand, we also question whether BB88’s field-giant relation between spectral type and V–I is correct. If we take the colors from this relation and plug them into the V–I,  $T_{\text{eff}}$  relation of Bessell (1998), we get an STT relation which differs significantly from that of DBBR, which we have used as the basis for our modelling of M giants. Thus, assuming that BB88’s V–I, spectral type relation is correct forces us to conclude that either the color-temperature relation of Bessell (1998) is wrong or that the STT relation of DBBR is in error. Without some additional information, we cannot resolve these discrepancies between the V–I, spectral type relations of field giants given by BB88 and Thé et al. (1990).

Figure 14 shows the comparisons for the V–K and J–K colors. In this figure, the color,  $T_{\text{eff}}$  relations of the field giants generally come from the same sources as the optical relations; the V–K,  $T_{\text{eff}}$  relation was published by Bessell et al. (1998). The color, spectral type data for the field stars is taken from BB88. The crosses again represent the photometry of FPTWWS; their ESO colors have been transformed to the Johnson-Glass system using the color transformations given by BB88. Since FPTWWS’s spectra only extended to  $9000 \text{ \AA}$ , near-infrared colors could not be measured from them.

The color most often used to determine effective temperatures of cool stars is V–K, so it would be gratifying if our models predicted the same V–K,  $T_{\text{eff}}$  relation as that observed in field M giants. This appears to hold true for spectral types earlier than about type M4, but the cooler models become progressively redder than the color-temperature relation of Bessell et al. (1998), reaching  $\sim 0.6$  mag redder at spectral type M7. However, the opposite holds true for the V–K, spectral type data. Here, the models are slightly bluer than the field relation (BB88) but overlap FPTWWS’s transformed photometry. The filled squares shown in the upper two panels of Figure 14 show the V–K colors of the models which result when the synthetic V–band magnitudes are “corrected” for their differences with the respective V magnitudes measured from the FPTWWS spectra; this approximates the V–K colors we would expect to measure from the FPTWWS spectra if their wavelength coverage included the K band. This adjustment makes the model colors an excellent match to the field stars in the color, spectral type plane but obviously makes the fit to the M-giant color-temperature relation much worse. However, we expect the synthetic V–K colors to be too red for spectral types M5 and later because we have neglected H<sub>2</sub>O absorption in our calculations; its inclusion would make the K magnitudes fainter but leave the V magnitudes unaffected. Since we encounter the same uncertainty here that we experienced in the V–I plots, namely that substituting the colors from BB88’s V–K, spectral type relation into Bessell et al. (1998)’s V–K,  $T_{\text{eff}}$  relation gives an STT relation which differs from that of DBBR, it is not clear to us which field relation (color-temperature or color-type) is more reliable. In either case, the model vs. field-star color differences are relatively small for the early-to-mid-M giants, so we are satisfied that our models provide an adequate representation of the V–K colors of field M giants to be used for evolutionary synthesis.

The J–K colors of the models match the field relations for the K giants but become slightly redder than the field relation of Gratton et al. (1996) at a given  $T_{\text{eff}}$  for early-M types. The models, however, are in excellent agreement with the J–K vs. spectral type relation of BB88 through spectral type M4. As mentioned in Section 3.1, we have not been able to calibrate the absorption bands of the  $\phi$ -system of TiO, some of which fall in the J band, using empirical spectra. Therefore, we allowed the J–K colors of the models to assist us in choosing a final  $f_{00}$  value for the  $\phi$  system, since the model J–K colors redden significantly as this parameter is increased. For the later M types, we expect that adding spectral lines of H<sub>2</sub>O to the synthetic spectrum calculations, while diminishing both the J-band and K-band fluxes, would resolve the remaining differences between the models and the field-giant relations.

In Figure 15, we compare the bolometric corrections of our models of field K and M giants, as a function of spectral type, to empirical relations. Recall that the BCs of the models assume  $M_{V,\odot} = +4.84$ ,  $BC_{V,\odot} = -0.12$ ,  $M_{K,\odot} = +3.31$  and  $BC_{K,\odot} = +1.41$ ; this

implies a  $(V-K)_{\text{CIT}}$  color for the Sun of 1.53, which is  $\sim 0.02$  mag redder than the best observed values tabulated by Bessell et al. (1998). In the upper panel of this figure, the open circles are the (untabulated) V-band BCs of our models, the solid line is the field relation of Johnson (1966), and the M-giant relation of Lee (1970) is shown as a dotted line. The two field relations are virtually identical and are in close agreement with the model BCs for spectral types K0–M3; at later types, the models predict  $BC_V$  values which are smaller in magnitude than the field relations imply. However, recall that our synthetic V-band magnitudes are probably too bright, due to missing opacity in the synthetic spectrum calculations. If we substitute the V-band magnitudes measured from the “intrinsic” MK M-giant spectra of FPTWWS into the  $BC_V$  calculations, then the model points move to the positions of the filled circles in the upper panel of Figure 15; the latter are a much better match to the field relations at late-M spectral types, showing that the differences between the field-star BCs and the model BCs are consistent with the corresponding differences in their observed and computed V magnitudes. It is precisely these uncertainties in the V-band magnitudes that led us to tabulate  $BC_K$  in Table 4 rather than  $BC_V$ .

In the lower panel of Figure 15, we compare our K-band bolometric corrections to some near-infrared field relations. Here, the open circles again represent our models, and the empirical trends have been calculated as prescribed by Bessell & Wood (1984). Bessell & Wood give relations between  $BC_K$  (on the CIT/CTIO system) and both  $(V-K)_{\text{CIT}}$  and  $(J-K)_{\text{AAO}}$ . Using the color transformation between  $(J-K)_{\text{CIT}}$  and  $(J-K)_{\text{AAO}}$  from BB88, we have used the calibrated, synthetic V–K and J–K colors of our models to calculate the  $BC_K$  values which the Bessell & Wood relations predict; the results are shown in the lower panel of Figure 15. The solid line comes from the model  $(V-K)_{\text{CIT}}$  colors, while the dashed line is produced when these colors are “corrected” for the differences between the V-band magnitudes of the models and those measured from the “intrinsic” M-giant spectra of FPTWWS. The dotted line results from the synthetic J–K colors when Bessell & Wood’s solar-metallicity J–K relation is used, while the crosses are the analogous points derived from their metal-poor relation. Surprisingly, the K-band BCs of the models better match the predicted BCs of metal-poor field stars of similar J–K color than those of their solar-metallicity counterparts. However, given the uncertainties in the calibration of the field-star  $BC_K$  vs. J–K relations and the nice agreement between the model BCs and those of field giants of similar V–K color, we can confidently recommend the use of our color-temperature relations and  $BC_K$  values of K and M giants for converting isochrones from  $\log T_{\text{eff}}$ ,  $\log L$  space into the color-magnitude plane.

#### 4.4. Color-Temperature Relations of M Giants

Given the generally good match between the broad-band colors and bolometric corrections measured from our synthetic spectra of field K and M giants and the empirical data, we have proceeded to construct grids of models of cool giants to supplement those presented in Paper I. At each of four metallicities, we have calculated MARCS model atmospheres and SSG synthetic spectra for stars having  $3000 \text{ K} \leq T_{\text{eff}} \leq 4000 \text{ K}$  and  $-0.5 \leq \log g \leq 1.5$ . Table 5 gives the calibrated colors and CIT/CTIO K-band bolometric corrections of these models; column 3 of Table 5 gives the spectral types measured from the synthetic spectra using the photometric system of Wing (1971). For those who are concerned about possible errors in the synthetic spectra due to missing opacity and/or spectral lines, we also provide Table 6, which gives the differences between the calibrated, synthetic V magnitudes and optical colors of our models of field M0–M7 giants and those measured from FPTWWS’s “intrinsic” M-giant spectra. The spectral types of the models can be used in conjunction with this table to “correct” the synthetic colors to match the observational data as desired, but we urge the reader to thoroughly review FPTWWS before adopting these color corrections. Also, keep in mind that the color calibrations have been derived from Population I stars, so the colors of the models having  $[\text{Fe}/\text{H}] \lesssim -0.5$  should be used with some degree of caution.

### 5. Conclusions

To better model elliptical galaxies through evolutionary synthesis, we have improved our synthetic spectra of M giants by 1) determining the optimal effective temperature scale to use for these cool stars, 2) adjusting the  $f_{00}$  values of the TiO bands to best match the band strengths observed in the spectra of field M giants, and 3) evaluating the resulting models by comparing the synthetic spectra, their estimated spectral types and the model colors and bolometric corrections to empirical data.

We have critically examined three effective temperature scales for M giants, each derived from angular diameter measurements. Two of these were taken from Dyck et al. (1996; DBBR) and Di Benedetto & Rabbia (1987); the third was derived from the angular diameters measured by Mozurkewich et al. (1991) and Mozurkewich (1997; M97 collectively). We found that the effective temperature vs. spectral type relation of Dyck et al. (1996) produces synthetic spectra which have the same continuous flux level as the “intrinsic” M giant spectrum of the same spectral type observed by Fluks et al. (1994). A possible exception to this rule occurs at spectral type M1, where the Dyck et al.  $T_{\text{eff}}$  may be a bit too cool. This temperature scale, which is similar to Di Benedetto

& Rabia’s but covers a wider range of spectral types, also proves to be a good match to that of Bell & Gustafsson (1989; BG89), which we adopted in a companion paper discussing color-temperature relations of hotter stars (Houdashelt et al. 2000). While the angular diameters measured by M97 were found to match those predicted by BG89 for G and K giants remarkably well, the resulting effective temperature scale could not be reliably extended into the M giant regime because his uniform-disk angular diameters were measured at 8000 Å. At this wavelength, TiO absorption is present in M star atmospheres, and the limb-darkening corrections used by Mozurkewich et al. (1991) did not take this into account.

Adopting DBBR’s effective temperature scale, we have constructed MARCS model atmospheres and SSG synthetic spectra for solar-metallicity K0–M7 giants. For each system of TiO, we adjusted the band absorption oscillator strength for the 0–0 transition,  $f_{00}$ , until we were best able to reproduce the “intrinsic” MK spectra of field M giants of Fluks et al. (1994). We found the resulting synthetic spectra to be a good match to the K-band spectra of Kleinmann & Hall (1986) as well. Quantitative measures of the spectral types of the M giant synthetic spectra based upon the strengths of both the TiO bands and the CO bandhead near 2.3  $\mu\text{m}$  are in good agreement with the spectral types expected from DBBR’s temperature scale. In addition, the broad-band colors of the K and M giant sequence are quite similar to those expected of solar-metallicity field stars of the same spectral type and/or  $T_{\text{eff}}$ , especially for the K and early-M stars. At later spectral types, most of the differences between the models and the empirical data can be ascribed to our omission of spectral lines of VO and H<sub>2</sub>O in the spectral synthesis.

Finally, we have presented colors and bolometric corrections for models having  $3000 \text{ K} \leq T_{\text{eff}} \leq 4000 \text{ K}$  and  $-0.5 \leq \log g \leq 1.5$  at four metallicities:  $[\text{Fe}/\text{H}] = +0.25, 0.0, -0.5$  and  $-1.0$ . These supplement and extend the color-temperature relations presented in our companion paper (Houdashelt et al. 2000).

We would like to thank the National Science Foundation (Grant AST93-14931) and NASA (Grant NAG53028) for their support of this research. We also thank Ben Dorman for allowing us to use his isochrone-construction code and Mike Bessell for providing many helpful suggestions on the manuscript. MLH would like to express his gratitude to Rosie Wyse for providing support while this work was completed. The research has made use of the Simbad database, operated at CDS, Strasbourg, France.

## REFERENCES

- Alvarez, R., & Plez, B. 1998, *A&A*, 330, 1109
- Baldwin, J. R., Frogel, J. A., & Persson, S. E. 1973, *ApJ*, 184, 427
- Bell, R. A., Branch, D. R., & Upson, W. 1976, *JQSRT*, 16, 177
- Bell, R. A., & Briley, M. M. 1991, *AJ*, 102, 763
- Bell, R. A., Dwivedi, P. H., Branch, D., & Huffaker, J. N. 1979, *ApJS*, 41, 593
- Bell, R. A., Eriksson, K., Gustafsson, B., & Nordlund, Å. 1976, *A&AS*, 23, 37
- Bell, R. A., & Gustafsson, B. 1978, *A&AS*, 34, 229
- Bell, R. A., & Gustafsson, B. 1989, *MNRAS*, 236, 653 (BG89)
- Bell, R. A., Paltoglou, G., & Tripicco, M. J. 1994, *MNRAS*, 268, 771
- Bell, R. A., & Tripicco, M. J. 1991, *AJ*, 102, 777
- Bessell, M. S. 1998, private communication
- Bessell, M. S., & Brett, J. M. 1988, *PASP*, 100, 1134 (BB88)
- Bessell, M. S., Brett, J. M., Scholz, M., & Wood, P. R. 1989a, *A&AS*, 77, 1
- Bessell, M. S., Brett, J. M., Scholz, M., & Wood, P. R. 1989b, *A&A*, 213, 209
- Bessell, M. S., Castelli, F., & Plez, B. 1998, *A&A*, 333, 231
- Bessell, M. S., & Wood, P. R. 1984, *PASP*, 96, 247
- Blanco, V. M. 1964, *AJ*, 69, 730
- Brett, J. M. 1990, *A&A*, 231, 440
- Brett, J. M. 1991, private communication
- Cohen, J. G., Frogel, J. A., & Persson, S. E. 1978, *ApJ*, 222, 165
- Cohen, J. G., Frogel, J. A., Persson, S. E., & Zinn, R. 1980, *ApJ*, 239, 74
- Cousins, A. W. J. 1980, *South African Astron. Obs. Circ.*, 1, 234
- Davis, S. P., Littleton, J. E., & Phillips, J. G. 1986, *ApJ*, 309, 449

- Di Benedetto, G. P. 1993, *A&A*, 270, 315 (DiB93)
- Di Benedetto, G. P., & Ferluga, S. 1990, 236, 449
- Di Benedetto, G. P., & Rabbia, Y. 1987, *A&A*, 188, 114 (DiBR)
- Dyck, H. M., Benson, G. T., van Belle, G. T., & Ridgway, S. T. 1996, *AJ*, 111, 1705 (DBBR)
- FitzGerald, M. P. 1969, *JRASC*, 63, 251
- Fluks, M. A., Plez, B., Thé, P. S., de Winter, D., Westerlund, B. E., & Steenman, H. C. 1994, *A&AS*, 105, 311 (FPTWWS)
- Frogel, J. A., Becklin, E. E., Neugebauer, G., Matthews, K., Persson, S. E., & Aaronson, M. 1975, *ApJ*, 195, L15
- Frogel, J. A., Persson, S. E., Aaronson, M., & Matthews, K. 1978, *ApJ*, 220, 75 (FPAM)
- Frogel, J. A., Persson, S. E., & Cohen, J. G. 1979, *ApJ*, 227, 499
- Frogel, J. A., Persson, S. E., & Cohen, J. G. 1980, *ApJ*, 240, 785
- Frogel, J. A., Persson, S. E., & Cohen, J. G. 1981, *ApJ*, 246, 842
- Frogel, J. A., Persson, S. E., & Cohen, J. G. 1983, *ApJS*, 53, 713
- Gratton, R. G., Carretta, E., & Castelli, F. 1996, *A&A*, 314, 191
- Gustafsson, B., & Bell, R. A. 1979, *A&A*, 74, 313
- Gustafsson, B., Bell, R. A., Eriksson, K., & Nordlund, Å. 1975, *A&A*, 42, 407
- Hedgecock, I. M., Naulin, C., & Costes, M. 1995, *A&A*, 304, 667
- Hoffleit, D., & Jaschek, C. 1982, *The Bright Star Catalogue* (New Haven: Yale Univ. Obs.)
- Houdashelt, M. L. 1995, Ph.D. thesis, Ohio State Univ.
- Houdashelt, M. L., Bell, R. A., & Sweigart, A. V. 2000, *AJ*, accepted (Paper I)
- Houdashelt, M. L., Bell, R. A., & Sweigart, A. V. 2001, in preparation
- Houk, N. 1978, *Michigan Catalogue of Two-Dimensional Spectral Types for the HD Stars*, Vol. 2 (Ann Arbor: Univ. Michigan Dept. Astron.)

- Houk, N. 1982, Michigan Catalogue of Two-Dimensional Spectral Types for the HD Stars, Vol. 3 (Ann Arbor: Univ. Michigan Dept. Astron.)
- Houk, N., & Cowley, A. P. 1975, Michigan Catalogue of Two-Dimensional Spectral Types for the HD Stars, Vol. 1 (Ann Arbor: Univ. Michigan Dept. Astron.)
- Johnson, H. L. 1966, ARA&A, 4, 193
- Jørgensen, U. G. 1994, A&A, 284, 179
- Keenan, P. C., & McNeil, R. C. 1976, An Atlas of Spectra of the Cooler Stars, Ohio State University Press.
- Kiehling, R. 1987, A&AS, 69, 465
- Kjærgaard, P., Gustafsson, B., Walker, G. A. H., & Hultqvist, L. 1982, A&A, 115, 145
- Kleinmann, S. G., & Hall, D. N. B. 1986, ApJS, 62, 501 (KH86)
- Kovacs, I. 1969, Rotational Structure in the Spectra of Diatomic Molecules (American Elsevier Publishing Co., New York)
- Langhoff, S. R. 1997, ApJ, 481, 1007
- Larsson, M. 1983, A&A, 128, 291
- Lee, T. A., 1970, ApJ, 162, 217
- Ludwig, C. B., Malkmus, W., Reardon, J. E., & Thomas, J. A. L. 1973, Handbook of Infrared Radiation from Combustion Gases (NASA SP-3080)
- MacConnell, D. J., Wing, R. F., & Costa, E. 1992, AJ, 104, 821
- Manduca, A. 1979, A&AS, 36, 411
- McWilliam, A., & Rich, R. M. 1994, ApJS, 91, 749
- Mikami, T. 1978, PASJ, 30, 191
- Mozurkewich, D. 1997, in Poster Proceedings of IAU Symposium 189 on Fundamental Stellar Properties: The Interaction Between Observation and Theory, ed. T. R. Bedding (Sydney: Univ. Sydney), 14 (M97)
- Mozurkewich, D., Johnston, K. J., Simon, R. S., Bowers, P. F., Gaume, R., Hutter, D. J., Colavita, M. M., Shao, M., & Pan, X. P. 1991, AJ, 101, 2207 (M97)

- Nassau, J. J., & Velghe, A. G. 1964, *ApJ*, 139, 190
- Perrin, G., Coudé du Foresto, V., Ridgway, S. T., Mariotti, J.-M., Traub, W. A., Carleton, N. P., & Lacasse, M. G. 1998, *A&A*, 331, 619
- Persson, S. E., Aaronson, M., & Frogel, J. A. 1977, *AJ*, 82, 729
- Persson, S. E., Cohen, J. G., Matthews, K., Frogel, J. A., & Aaronson, M. 1979, *ApJ*, 235, 452
- Persson, S. E., Cohen, J. G., Matthews, K., Frogel, J. A., & Aaronson, M. 1983, *ApJ*, 266, 105
- Persson, S. E., Cohen, J. G., Sellgren, K., Mould, J., & Frogel, J. A. 1980, *ApJ*, 240, 779
- Phillips, J. G. 1973, *ApJS*, 26, 313
- Plez, B. 1996, private communication
- Plez, B. 1998, private communication
- Plez, B., Brett, J. M., & Nordlund, Å. 1992, *A&A*, 256, 551
- Ramírez, S. V., DePoy, D. L., Frogel, J. A., Sellgren, K., & Blum, R. D. 1997, *AJ*, 113, 1411 (RDFSB)
- Ridgway, S. T., Joyce, R. R., White, N. M., & Wing, R. F. 1980, *ApJ*, 235, 126
- Scholz, M. 1985, *A&A*, 145, 251
- Scholz, M., & Takeda, Y. 1987, *A&A*, 186, 200
- Scholz, M., & Tsuji, T. 1984, *A&A*, 130, 11
- Scholz, M., & Wehrse, R. 1982, *MNRAS*, 200, 41
- Schryber, J. H., Miller, S., & Tennyson, J. 1995, *JQSRT*, 53, 373
- Smith, V. V., & Lambert, D. L. 1990, *ApJS*, 72, 387
- Terndrup, D. M., Frogel, J. A., & Whitford, A. E. 1990, *ApJ*, 357, 453 (TFW)
- Terndrup, D. M., Frogel, J. A. & Whitford, A. E. 1991, *ApJ*, 378, 742
- Thé, P. S., Thomas, D., Christensen, C. G., & Westerlund, B. E. 1990, *PASP*, 102, 565

Wing, R. F. 1971, in Proceedings of the Conference on Late-Type Stars, ed. G. W. Lockwood, & H. M. Dyck, 145

Wing, R. F., & Yorke, S. B. 1979, in IAU Colloq. 47, Spectral Classification of the Future, ed. M. F. McCarthy, A. G. D. Philip, and G. V. Coyne (Vatican City: Ricerche Astronomiche), 519

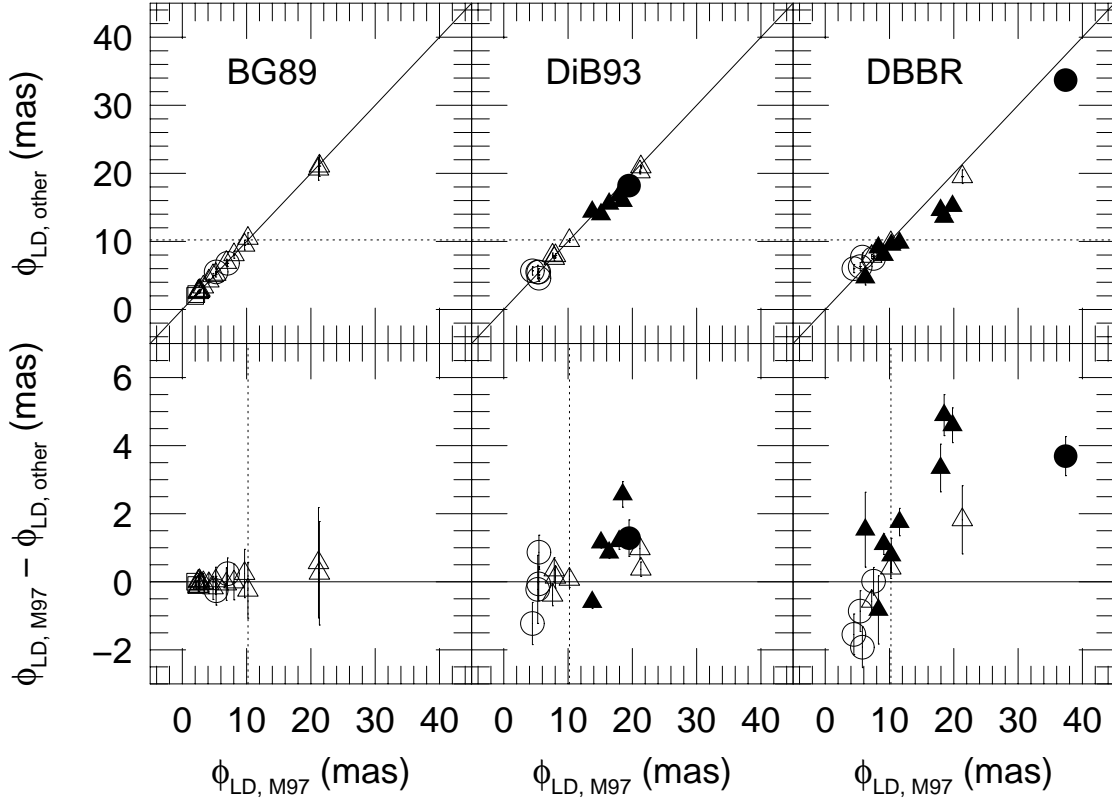


Fig. 1.— Comparison of limb-darkened angular diameter measurements ( $\phi_{LD}$ ) of G–M stars. The upper panels show direct comparisons of the  $\phi_{LD}$  measurements; the lower panels show the  $\phi_{LD}$  differences. From left to right, the following comparisons are made: Bell & Gustafsson (1989; BG89) vs. Mozurkewich et al. (1991) and Mozurkewich (1997; M97 collectively), Di Benedetto (1993; DiB93) vs. M97, and Dyck et al. (1996; DBBR) vs. M97. The error bars for the M97, DiB93 and DBBR angular diameters come directly from the respective references; those for the BG89 diameters were calculated as described in the text. Solid lines show equality of the diameters. Dotted lines appear at 10.22 mas; DBBR noted systematic differences between their diameters and those of Di Benedetto & Rabbia (1987) for stars larger than this. Supergiants, giants and subgiants are shown as circles, triangles and squares, respectively; open symbols are G and K stars, and filled symbols are M stars.

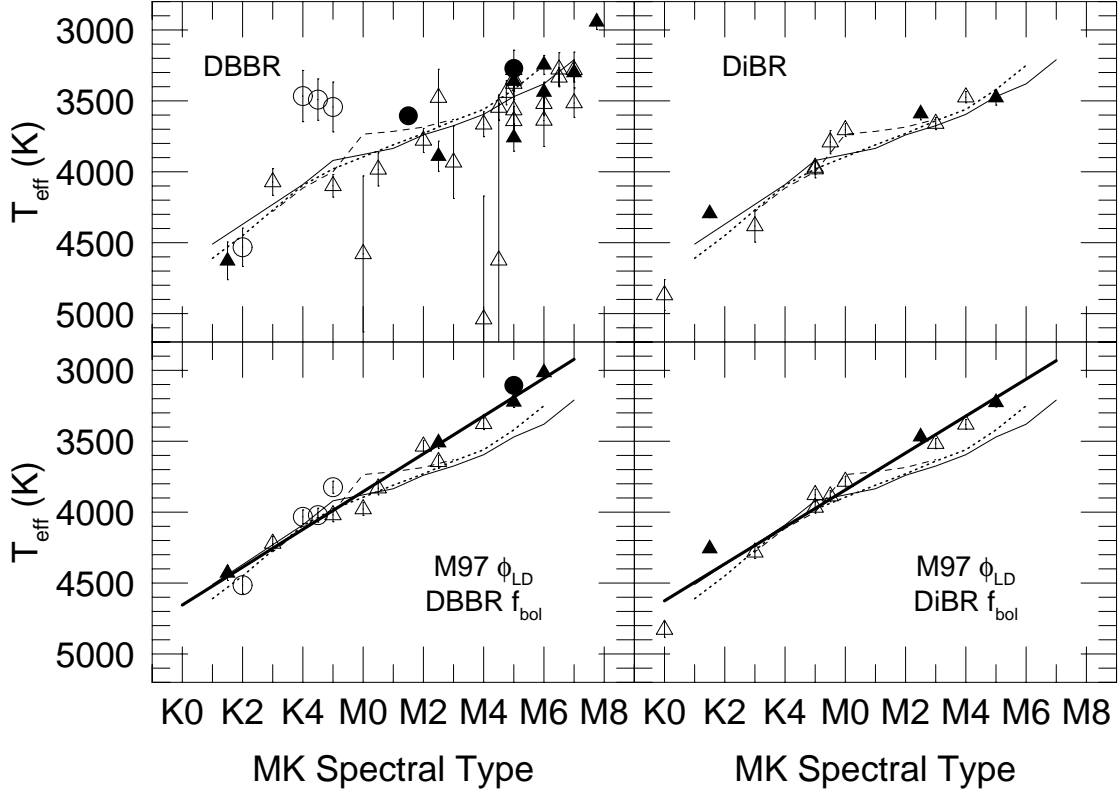


Fig. 2.— Spectral type, effective temperature relations for K–M giants. The upper, left-hand and upper, right-hand panels show the data (and error bars) reported by Dyck et al. (1996; DBBR) and Di Benedetto & Rabbia (1987; DiBR), respectively. The lower panels show the effective temperatures which result when the angular diameters of Mozurkewich et al. (1991) and Mozurkewich (1997; M97 collectively) are substituted for those of DBBR and DiBR in the  $T_{\text{eff}}$  calculations of the stars in the respective upper panels which M97 observed. The calculation of the temperature errors for these data is described in the text. Supergiants are represented by circles, and giants are triangles. Open symbols are stars with  $\phi_{\text{UD}} < 10$  mas; filled symbols are larger stars. The solid, dotted and dashed lines in each panel show the relations tabulated by DBBR, Ridgway et al. (1980) and DiBR, respectively. The bold lines in the lower panels are linear, least-squares fits to the data shown there.

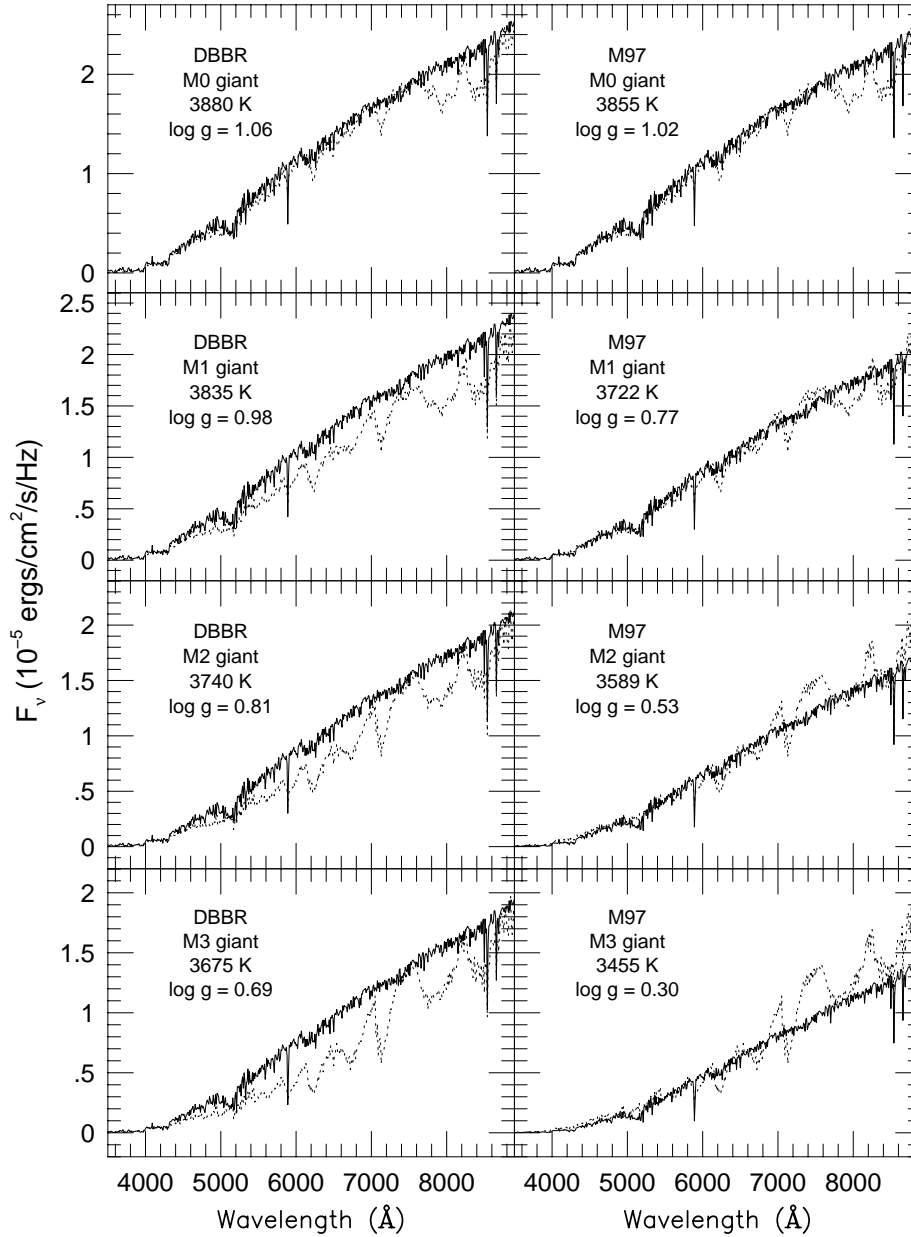


Fig. 3.— Comparisons of field-star spectra of M0–M3 giants and our synthetic spectra which omit spectral lines of TiO. The solid lines are the solar-metallicity synthetic spectra, and the dotted lines are the “intrinsic” MK spectra of field M giants from Fluks et al. (1994). The left-hand panels show synthetic spectra calculated assuming the  $T_{\text{eff}}$ , spectral type relation of Dyck et al. (1996; DBBR), and the synthetic spectra in the right-hand panels result from the relation derived here using the angular diameter measurements of Mozurkewich et al. (1991) and Mozurkewich (1997; collectively M97). The Fluks et al. spectra are the same in adjacent left-hand and right-hand panels. All panels are labeled with the temperature relation adopted, the spectral type of the Fluks et al. spectrum and the  $T_{\text{eff}}$  and  $\log g$  values used in the corresponding models.

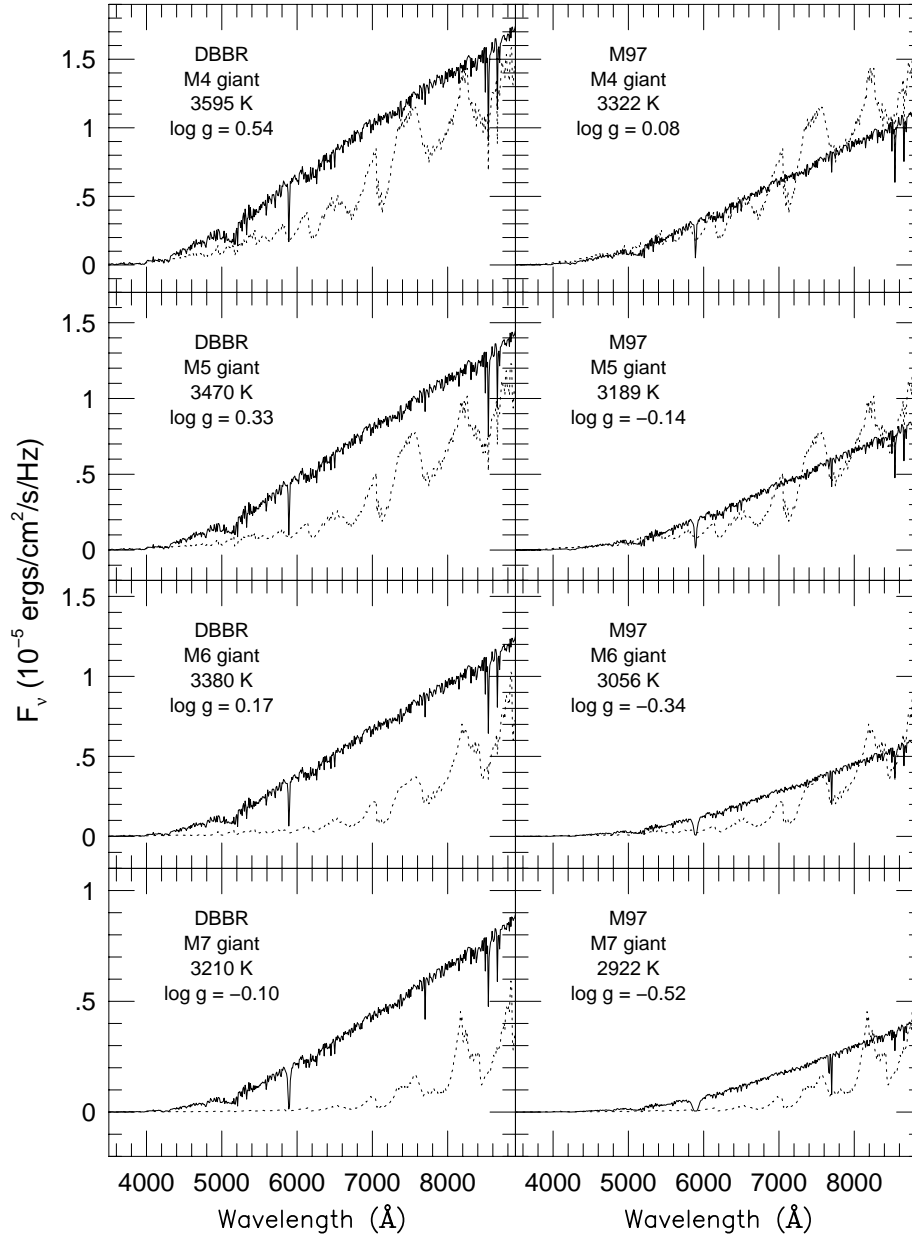


Fig. 4.— Comparisons of field-star spectra of M4–M7 giants and our synthetic spectra which omit spectral lines of TiO. See the caption to Figure 3 for further details.

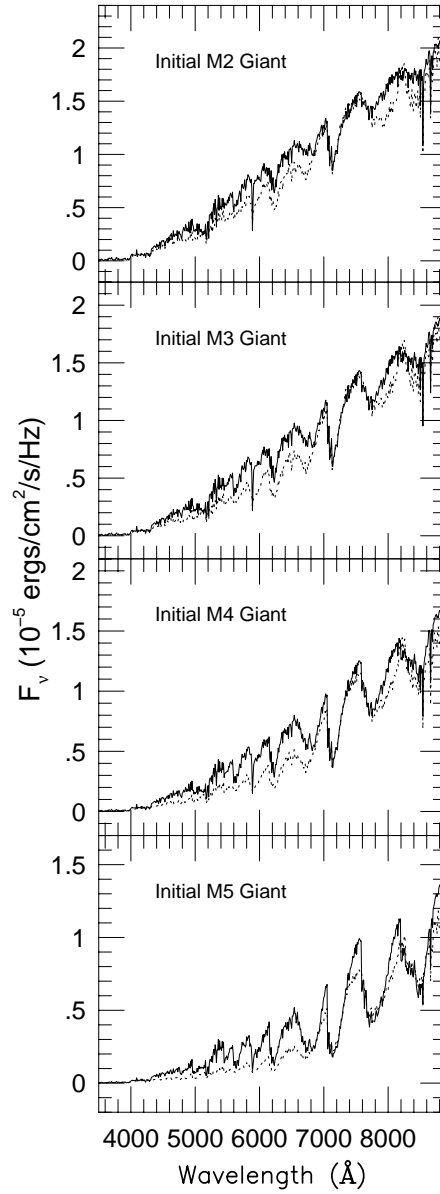


Fig. 5.— Comparisons of field-star spectra of M2–M5 giants and our synthetic spectra which were calculated with our original molecular data for TiO. The solid lines are the solar-metallicity synthetic spectra, and the dotted lines are the “intrinsic” MK spectra of field M giants from Fluks et al. (1994).

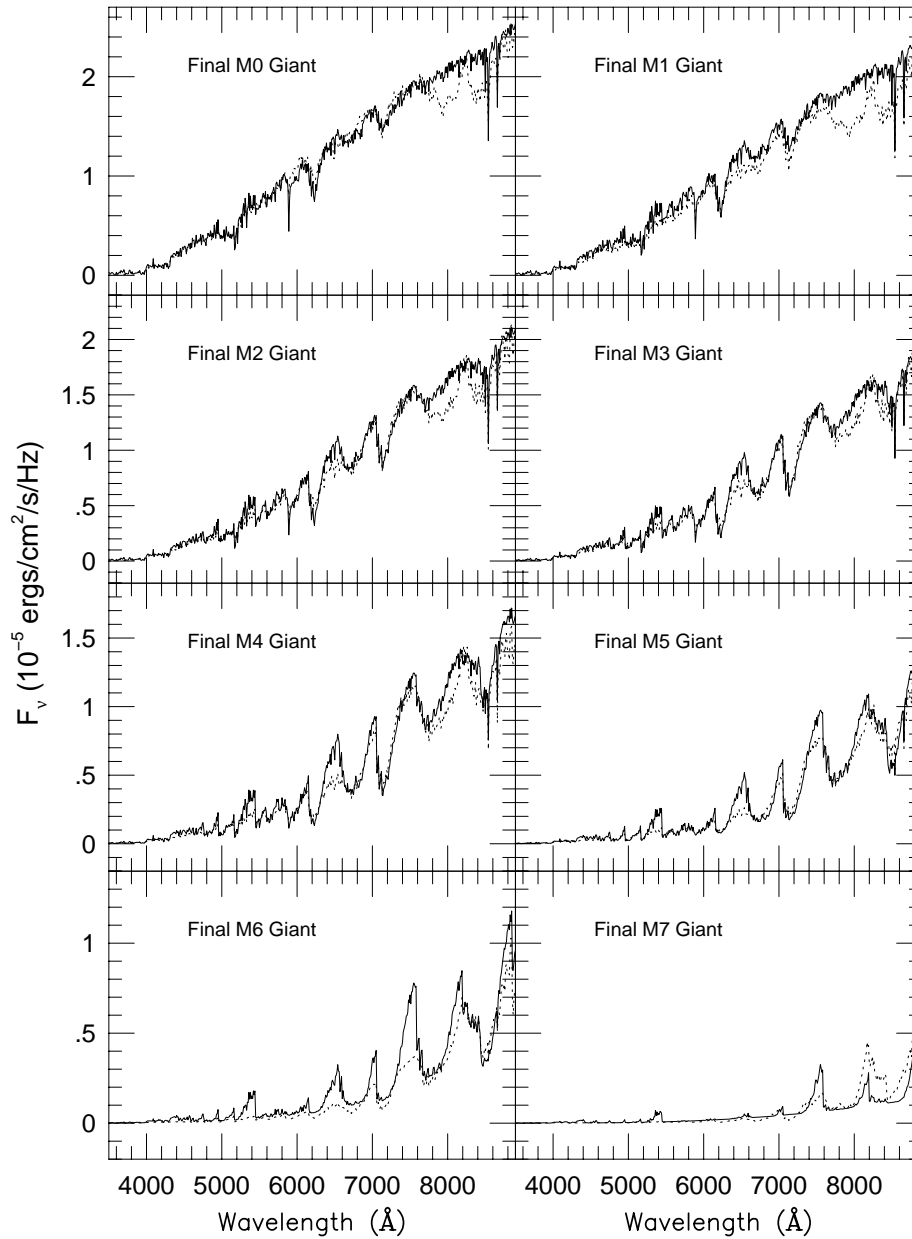


Fig. 6.— Comparisons of field-star spectra of M0–M7 giants and our synthetic spectra which were calculated with our revised molecular data for TiO. The solid lines are the solar-metallicity synthetic spectra, and the dotted lines are the “intrinsic” MK spectra of field M giants from Fluks et al. (1994).

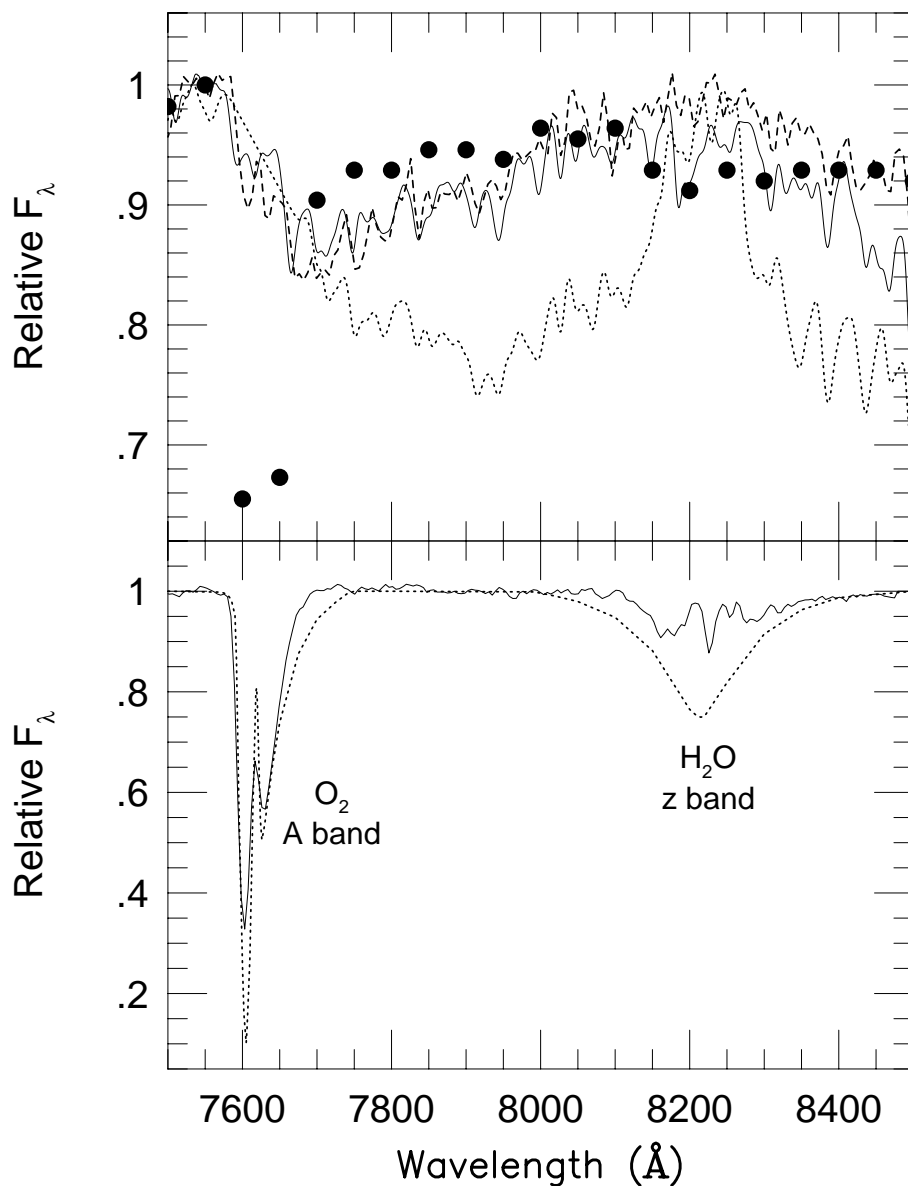


Fig. 7.— Illustration of the possible flux calibration error in the Fluks et al. (1994) “intrinsic” spectra. The upper panel compares the M2 giant spectrum of Fluks et al. (dotted line) to the analogous synthetic spectrum (solid line), the spectrum of HD 100783 (dashed line), a field M2 giant observed by Terndrup et al. (1990), and the spectrum of HR 4517 (points), a field M1 giant observed by Kiehling (1987); the Fluks et al. spectrum and the synthetic spectrum have been convolved to the resolution of the Terndrup et al. data, and all of the spectra have been normalized near 7532 Å. In the lower panel, the telluric corrections applied to the observational data by Fluks et al. (dotted line) and to the HD 100783 spectrum by Houdashelt (1995; solid line) are shown; Kiehling’s spectrum has not been corrected for telluric absorption.

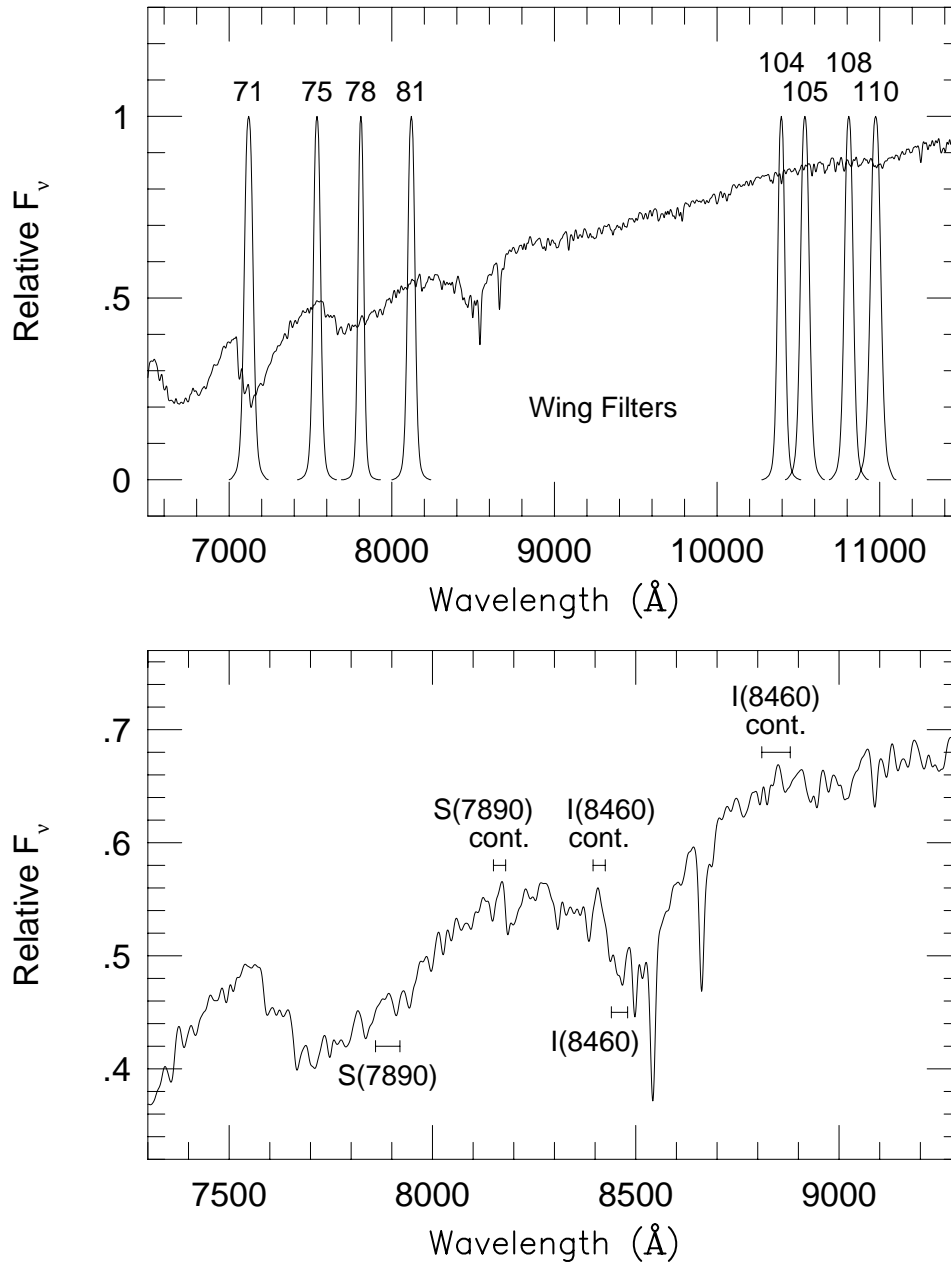


Fig. 8.— The systems used to estimate spectral types from TiO bands in the synthetic spectra. In the upper panel, the filter profiles of Wing’s (1971) photometric system overlay our synthetic spectrum of an M3 giant. In the lower panel, the bandpasses used to define the S(7890) and I(8460) indices of Terndrup et al. (1990), which measure pseudo-equivalent widths of TiO, are shown along with the same synthetic spectrum which appears in the upper panel.

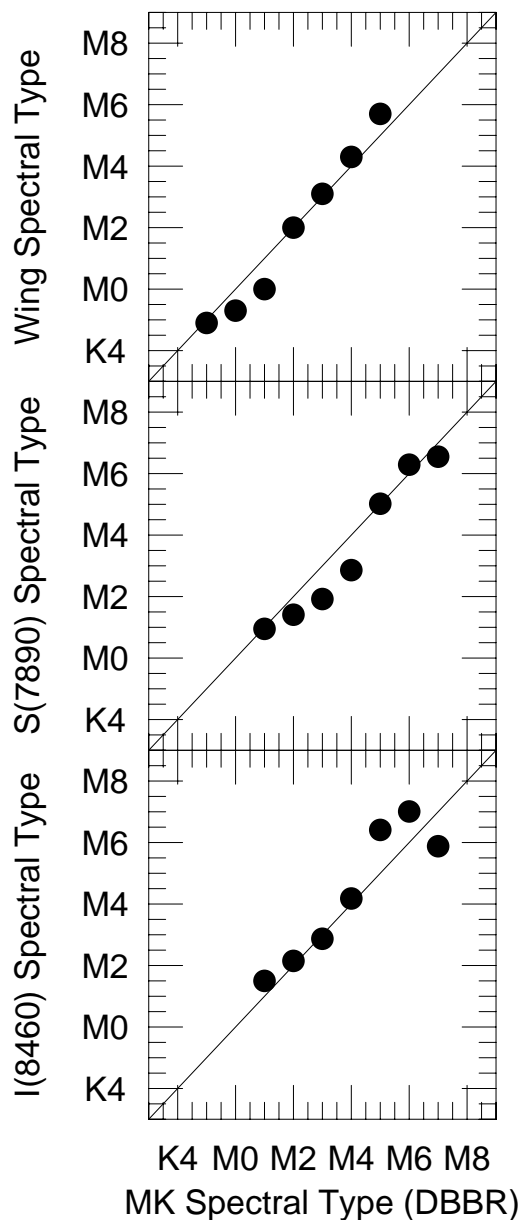


Fig. 9.— Comparison of the spectral types measured from the TiO bands of the synthetic spectra and those indicated by their effective temperatures (DBBR). Solid lines show equality of the two spectral type estimates in all panels. The spectral types have been measured from the synthetic spectra using Wing’s (1971) photometric system (upper panel), adopting the methodology of MacConnell et al. (1992); the S(7890) spectral index of Terndrup et al. (1990, center panel), using the the spectral type calibration derived by Houdashelt (1995); and the I(8460) index of Terndrup et al. (lower panel), using another of Houdashelt’s calibrations.

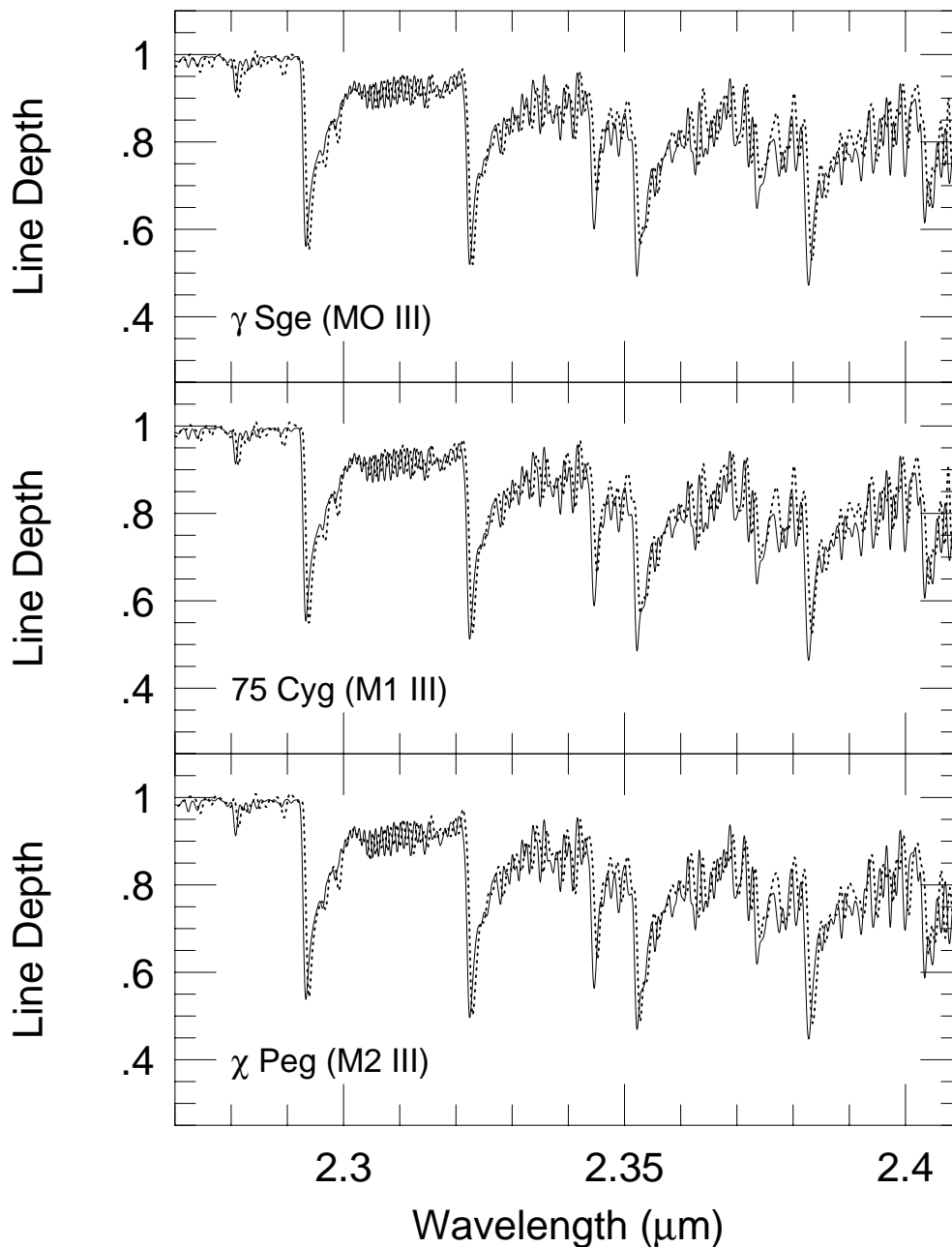


Fig. 10.— Comparisons of our synthetic spectra and the K-band spectra of field M giants observed by Kleinmann & Hall (1986; KH86). The bandhead of the  $^{12}\text{CO}(2,0)$  band is seen near  $2.292 \mu\text{m}$ . The solid lines represent the synthetic spectra, and the dotted lines are the KH86 spectra. The synthetic spectra have been convolved to the resolution of the KH86 data and rebinned to  $1.0 \text{ \AA}$  pixels. The slight wavelength difference between the empirical and synthetic spectra occurs because the observed spectra are calibrated using vacuum wavelengths, while the spectral line lists used to calculate the synthetic spectra use wavelengths in air.

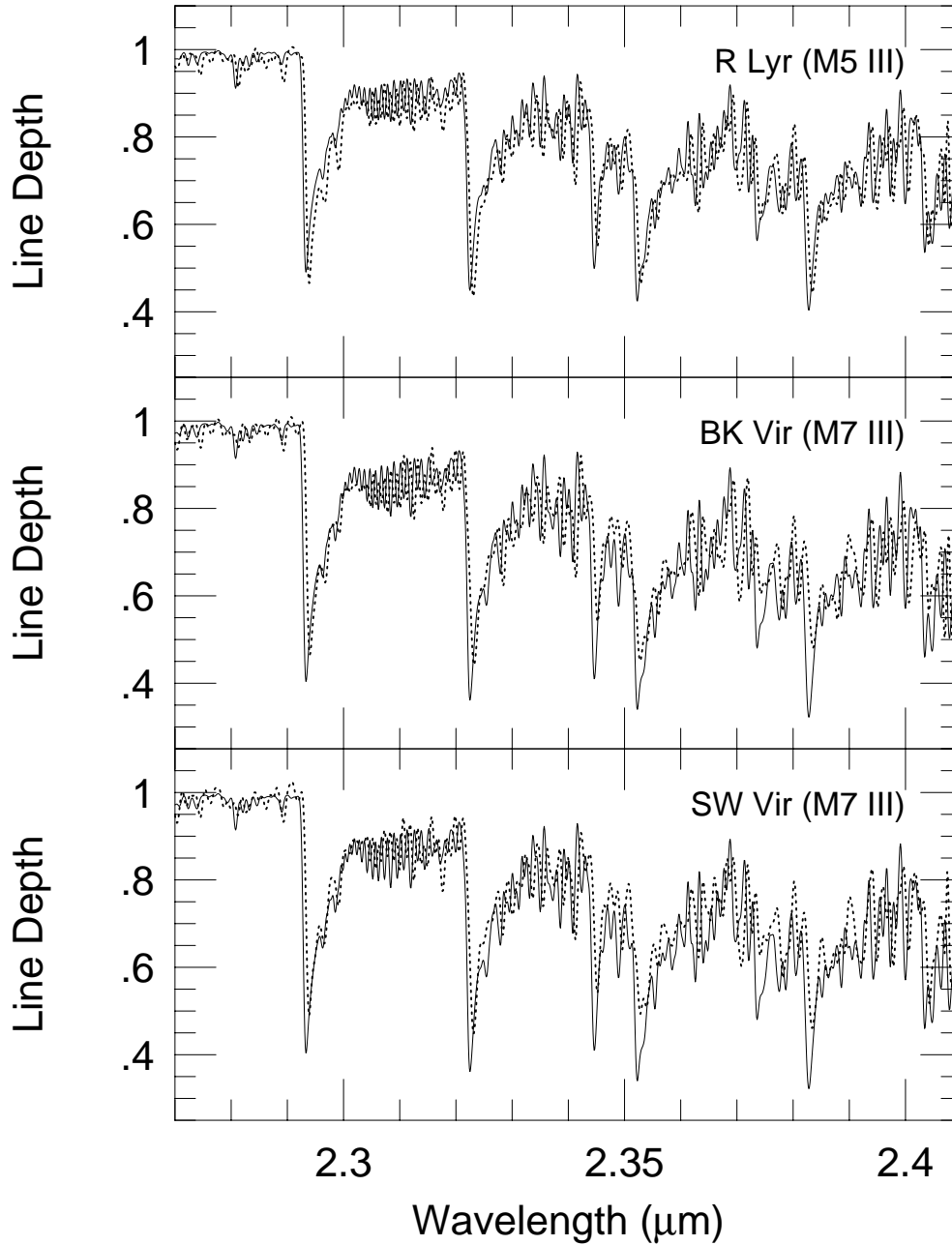


Fig. 11.— Further comparisons of our synthetic spectra and the K-band spectra of field M giants observed by Kleinmann & Hall (1986). The bandhead of the  $^{12}\text{CO}(2,0)$  band is seen near 2.292  $\mu\text{m}$ . See the caption to Figure 10 for further details.

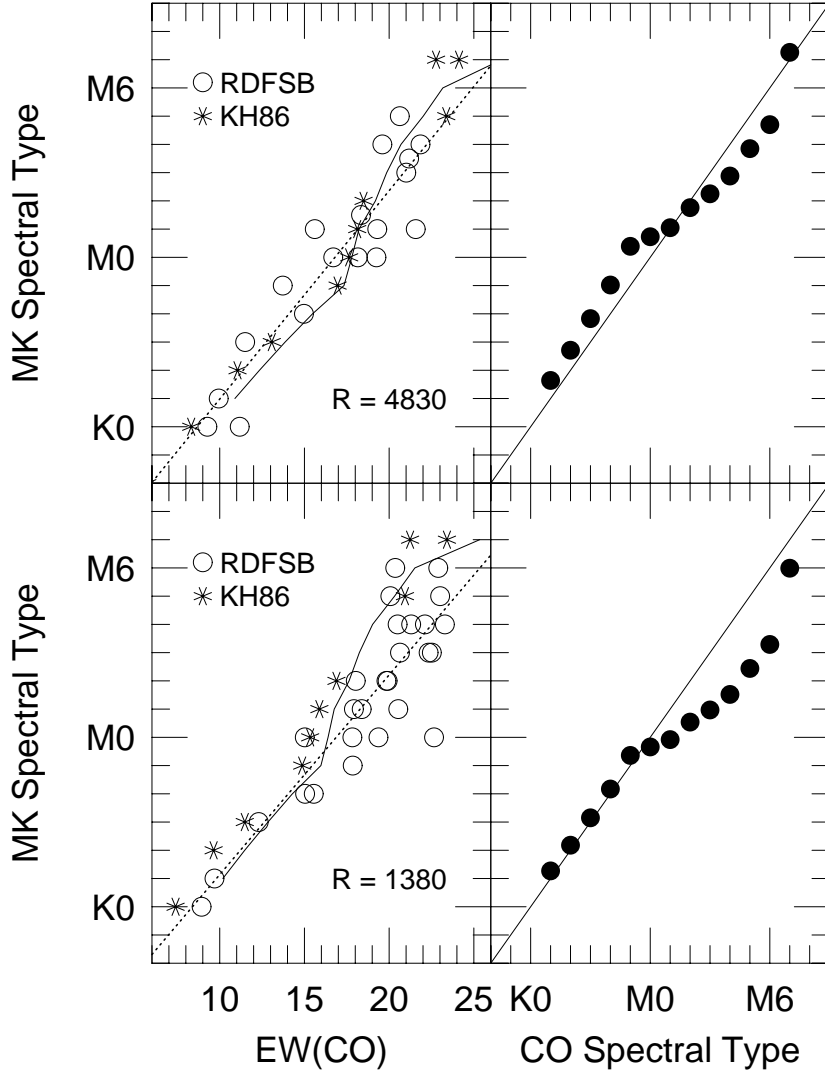


Fig. 12.— Comparison of the spectral types measured from the CO bands of the synthetic spectra and those indicated by their effective temperatures.  $EW(CO)$  measures the depth of the CO bandhead near  $2.3 \mu\text{m}$  using passbands defined by Ramírez et al. (1997; RDFSB); the continuum passbands used are resolution-dependent. The upper panels show comparisons at a resolution,  $R$ , of 4830, the lower panels at  $R=1380$ . In the left-hand panels, which show the relationship between  $EW(CO)$  and spectral type, open circles represent the  $EW(CO)$  measurements of RDFSB, and the dotted lines are linear, least-squares fits to this data. The asterisks show  $EW(CO)$  measured from the Kleinmann & Hall (1986; KH86) spectra using the appropriate continuum-band definitions, and the solid lines connect the measurements of  $EW(CO)$  from our synthetic spectra, after convolving and rebinning them to the resolution and dispersion of the corresponding RDFSB spectra. In the right-hand panels, the spectral types estimated from the synthetic  $EW(CO)$  values (using the dotted relations shown in the left-hand panels) are compared to the spectral types indicated by the effective temperatures of the models; the solid lines here represent equality of the two spectral type estimates.

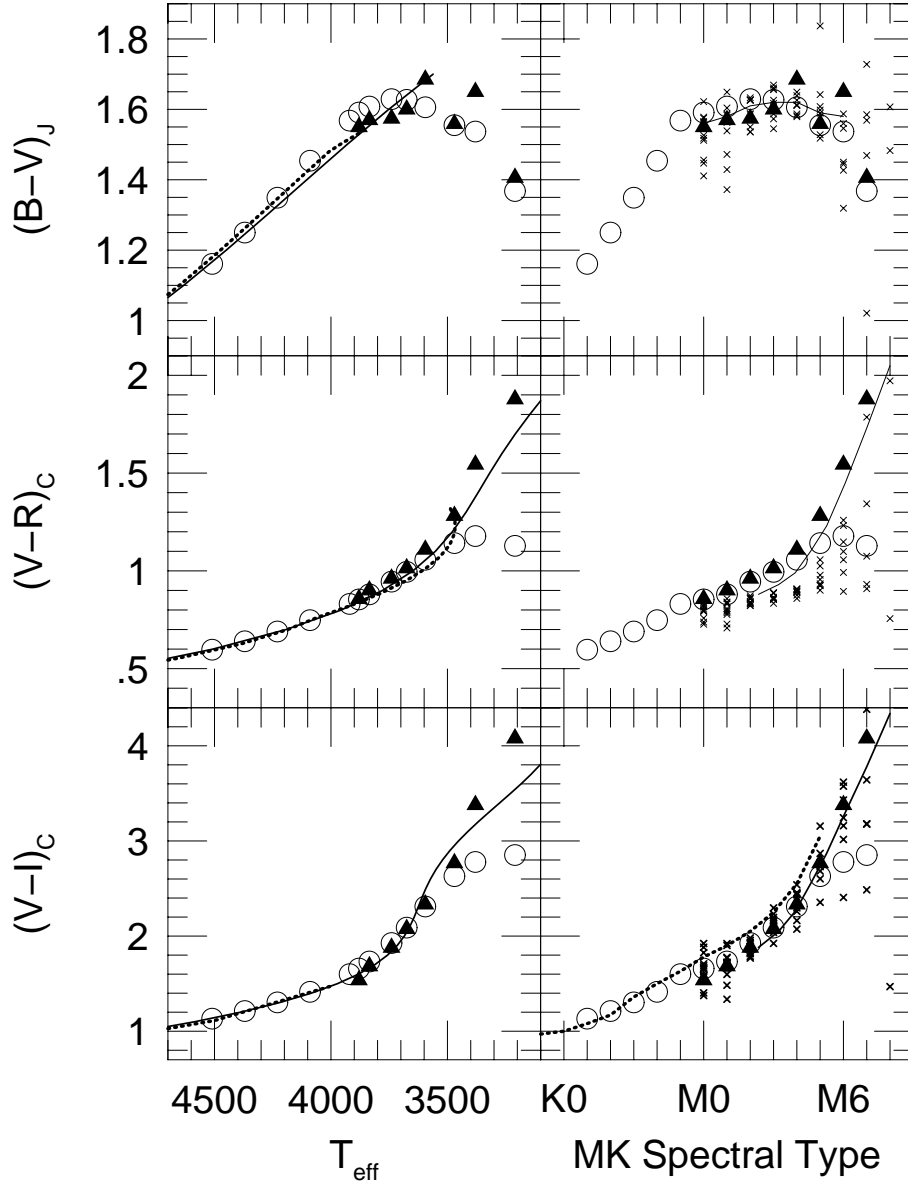


Fig. 13.— The calibrated, optical colors of the K and M giant models are compared to field-giant color,  $T_{\text{eff}}$  and color, spectral type relations. The left-hand panels show the color, temperature comparisons; the right-hand panels are color vs. spectral type. In all panels, the solid and dotted lines are the field-star relations, the open circles represent our models, the filled triangles show colors measured from the “intrinsic” MK spectra of Fluks et al. (1994), and the small crosses are the photometry of field M giants reported by Fluks et al. The field relations for color vs.  $T_{\text{eff}}$  have been taken from Bessell (1998; solid lines) and Gratton et al. (1996; dotted lines). The color, spectral type field relations come from Lee (1970) for B-V, Thé et al. (1990) for V-R and V-I (solid lines) and Bessell & Brett (1988) for V-I (dotted line). The Case spectral types of Thé et al. have been converted to MK types using the transformation given by Fluks et al.

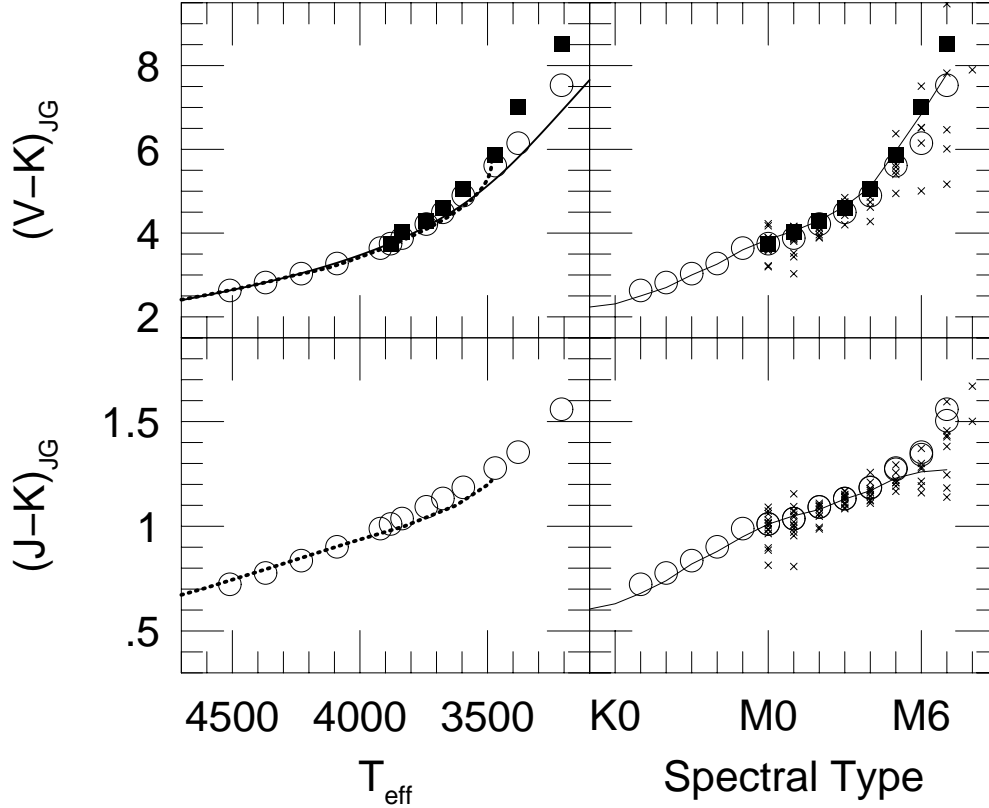


Fig. 14.— The calibrated V–K and J–K colors of the K and M giant models are compared to field-giant color,  $T_{\text{eff}}$  and color, spectral type relations. The left-hand panels show the color, temperature comparisons; the right-hand panels are color vs. spectral type. In all panels, the solid and dotted lines are the field star relations, the open circles represent our models, and the small crosses are the photometry of field M giants reported by Fluks et al. (1994). Fluks et al.’s photometry has been transformed from the ESO to the Johnson-Glass system using the color transformations given by Bessell & Brett (1988). The field relations for color vs.  $T_{\text{eff}}$  have been taken from Bessell et al. (1998; solid line) and Gratton et al. (1996; dotted lines). The color, spectral type field relations come from Bessell & Brett. The filled squares in the upper panels show the synthetic V–K colors which result when the V-band magnitudes of the models are “corrected” for the missing opacity indicated by the V magnitudes measured from the corresponding Fluks et al. spectra.

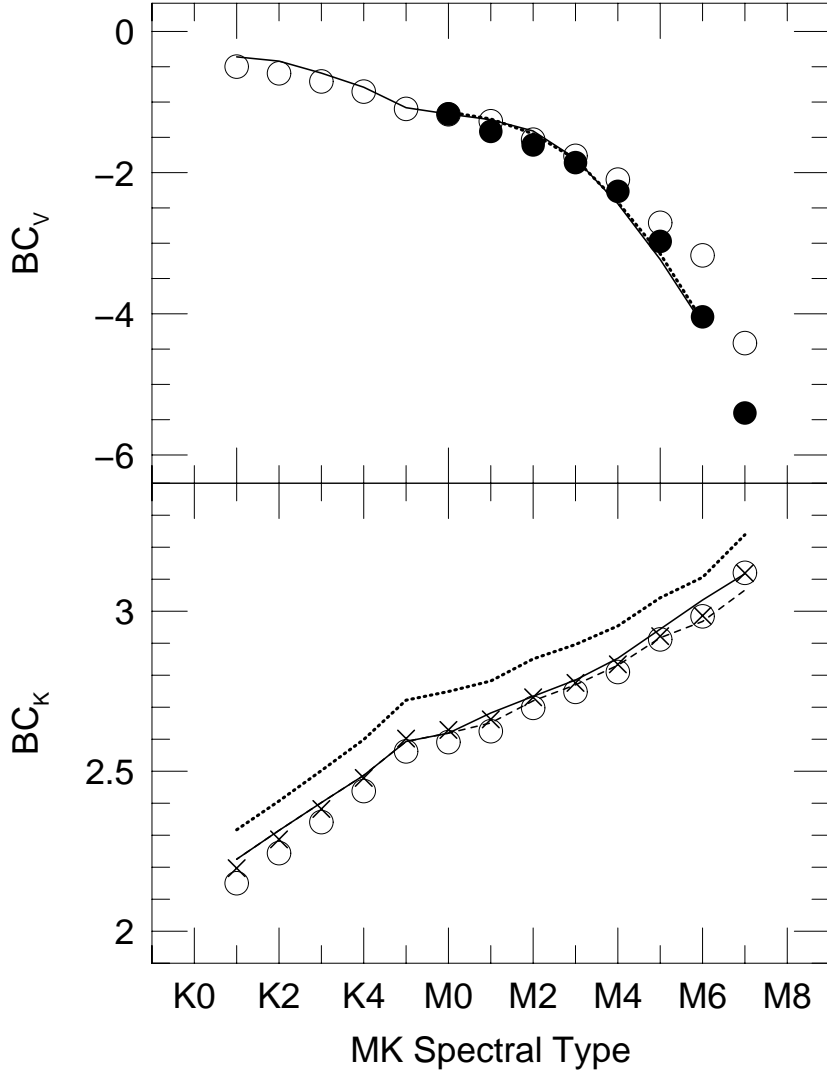


Fig. 15.— The bolometric corrections (BCs) of the K and M giant models are compared to those of field giants. The model BCs are shown as open circles. In the upper panel, the field-giant  $BC_V$ , spectral type relation of Johnson (1966) is shown as a solid line; that of Lee (1970) is a dotted line. The filled circles show the BCs of the models if the synthetic V-band magnitudes are “corrected” for their differences with the V magnitudes measured from the “intrinsic” MK spectra of field M giants of Fluks et al. (1994). The bottom panel compares the model CIT/CTIO  $BC_K$  values to those predicted for field giants of the same color using the relations of Bessell & Wood (1984). The solid and dashed lines are derived from the synthetic  $(V-K)_{\text{CIT}}$  colors; the latter results after “correcting” the V magnitudes of the models for their differences with the empirical data. The dotted line and crosses are derived from the synthetic  $(J-K)_{\text{CIT}}$  colors, after transforming them to the AAO system using the color transformation of Bessell & Brett (1988); the former comes from Bessell & Wood’s solar-metallicity relation, while the latter result when their relation for metal-poor stars is used instead.

TABLE 1. Comparison of Angular Diameter Measurements

Sample	M97 – BG89			M97 – DBBR			M97 – DiB93		
	$\langle\Delta\phi_{LD}\rangle^a$	s.d. <sup>b</sup>	n <sup>c</sup>	$\langle\Delta\phi_{LD}\rangle^a$	s.d. <sup>b</sup>	n <sup>c</sup>	$\langle\Delta\phi_{LD}\rangle^a$	s.d. <sup>b</sup>	n <sup>c</sup>
all stars	+0.006	0.194	20	+1.138	2.125	16	+0.457	0.910	16
subgiants	-0.047	0.069	2	...	...	...	...	...	...
giants	+0.015	0.196	16	+1.711	1.892	11	+0.607	0.880	11
supergiants	-0.013	0.354	2	-0.124	2.257	5	+0.128	0.984	5
G & K stars	+0.006	0.194	20	-0.380	1.266	7	+0.086	0.634	10
M stars	...	...	...	+2.318	1.919	9	+1.076	1.012	6
$\phi_{UD} < 10$ mas	-0.039	0.135	18	-0.013	1.235	11	-0.060	0.607	8
$\phi_{UD} > 10$ mas	+0.406	0.218	2	+3.670	1.214	5	+0.975	0.890	8

<sup>a</sup>Mean angular diameter difference.

<sup>b</sup>Standard deviation of the mean.

<sup>c</sup>Number of stars used to compute the mean.

References for Table 1.

M97 = Mozurkewich et al. (1991) and Mozurkewich (1997); BG89 = Bell & Gustafsson (1989); DBBR = Dyck et al. (1996); DiB93 = Di Benedetto (1993)

TABLE 2. Comparison of Giant-Star Effective Temperature Scales

Spectral Type	DBBR $T_{\text{eff}}$ (log g)	M97 $T_{\text{eff}}$ (log g)
K1	4510 (+2.29)	4522 (+2.32)
K2	4370 (+2.01)	4388 (+2.05)
K3	4230 (+1.74)	4255 (+1.79)
K4	4090 (+1.46)	4122 (+1.53)
K5	3920 (+1.14)	3988 (+1.27)
M0	3880 <sup>a</sup> (+1.06)	3855 (+1.02)
M1	3835 (+0.98)	3722 (+0.77)
M2	3740 (+0.81)	3589 (+0.53)
M3	3675 (+0.69)	3455 (+0.30)
M4	3595 (+0.54)	3322 (+0.08)
M5	3470 (+0.33)	3189 (−0.14)
M6	3380 (+0.17)	3056 (−0.34)
M7	3210 (−0.10)	2922 (−0.52)

<sup>a</sup>Interpolated from  $T_{\text{eff}}$  values for spectral types K5 and M1

References for Table 2.

DBBR = Dyck et al. (1996); M97 = Mozurkewich et al. (1991) and Mozurkewich (1997)

TABLE 3. Comparison of  $f_{00}$  Values of TiO Absorption Systems

System	DLP	B90 <sup>a</sup>	J94 <sup>a</sup>	HNC	L97	AP98 <sup>a</sup>	HBS
$\alpha$ ( $C^3\Delta-X^3\Delta$ )	0.031 <sup>b</sup>	0.041	0.07	0.043	0.0431	0.0435	0.408
$\beta$ ( $c^1\Phi-a^1\Delta$ )	0.26	0.14	0.26	0.11	0.1609	0.114	0.151
$\gamma$ ( $A^3\Phi-X^3\Delta$ )	0.12 <sup>b</sup>	0.065	0.11	0.057	0.0658	0.0565	0.0535
$\gamma'$ ( $B^3\Pi-X^3\Delta$ )	0.10	0.058	0.10	0.065	0.0781	0.0678	0.341
$\delta$ ( $b^1\Pi-a^1\Delta$ )	0.039	0.016	0.038	...	0.0753	0.038	0.00951
$\phi$ ( $b^1\Pi-d^1\Sigma$ )	0.03	0.012	0.031	...	0.0106	0.0107	0.000153
$\epsilon$ ( $E^3\Pi-X^3\Delta$ )	...	0.0021	0.012	<0.0047	0.0020	0.0020	0.0083 <sup>a</sup>

<sup>a</sup>Calculated from  $f_e$  using the  $q_{00}$  values of Langhoff (1997).

<sup>b</sup>See Jørgensen (1994).

References for Table 3.

DLP = Davis et al. (1986); B90 = Brett (1990); J94 = Jørgensen (1994); HNC = Hedgecock et al. (1995); L97 = Langhoff (1997); AP98 = Alvarez & Plez (1998); HBS = this paper.

TABLE 4. Calibrated Colors of Solar-Metallicity K0–M7 III Models

Type	$T_{\text{eff}}$	$\log g$	Johnson-Cousins				Johnson-Glass			CIT/CTIO				
			U-V	B-V	V-R	V-I	V-K	J-K	H-K	V-K	J-K	H-K	CO <sup>a</sup>	BC <sub>K</sub> <sup>b</sup>
K1	4510	2.29	2.292	1.161	0.597	1.132	2.631	0.723	0.112	2.648	0.667	0.108	0.125	2.150
K2	4370	2.01	2.569	1.250	0.640	1.212	2.820	0.777	0.124	2.837	0.717	0.120	0.145	2.244
K3	4230	1.74	2.868	1.349	0.690	1.303	3.032	0.836	0.140	3.049	0.772	0.137	0.166	2.341
K4	4090	1.46	3.185	1.454	0.748	1.414	3.274	0.902	0.160	3.290	0.832	0.155	0.189	2.438
K5	3920	1.14	3.529	1.568	0.831	1.600	3.642	0.989	0.191	3.659	0.914	0.185	0.216	2.562
M0	3880	1.06	3.600	1.591	0.854	1.659	3.748	1.011	0.199	3.764	0.933	0.193	0.223	2.591
M1	3835	0.98	3.657	1.608	0.880	1.733	3.882	1.037	0.207	3.897	0.957	0.201	0.230	2.625
M2	3740	0.81	3.723	1.629	0.945	1.927	4.216	1.093	0.229	4.231	1.009	0.223	0.245	2.698
M3	3675	0.69	3.714	1.627	0.995	2.089	4.497	1.133	0.245	4.510	1.045	0.238	0.256	2.748
M4	3595	0.54	3.637	1.606	1.057	2.311	4.897	1.186	0.266	4.909	1.094	0.258	0.270	2.810
M5	3470	0.33	3.401	1.555	1.142	2.630	5.612	1.278	0.302	5.623	1.177	0.292	0.291	2.912
M6	3380	0.17	3.234	1.537	1.178	2.779	6.147	1.354	0.330	6.156	1.245	0.319	0.311	2.984
M7	3210	-0.10	2.704	1.368	1.128	2.852	7.531	1.559	0.396	7.535	1.426	0.383	0.366	3.120

<sup>a</sup>No color calibration applied; see Paper I.

<sup>b</sup>BC<sub>V</sub> = BC<sub>K</sub> - (V-K).

TABLE 5. Calibrated Color-Temperature Relations of M Giants

$T_{\text{eff}}/\log g/[\text{Fe}/\text{H}]$	Type <sup>a</sup>	Johnson-Cousins				Johnson-Glass			CIT/CTIO				
		U-V	B-V	V-R	V-I	V-K	J-K	H-K	V-K	J-K	H-K	CO <sup>b</sup>	BC <sub>K</sub> <sup>c</sup>
4000/-0.50/+0.25	<K4	4.676	1.855	0.853	1.534	3.385	0.844	0.244	3.405	0.781	0.243	0.320	2.490
4000/0.00/+0.25	K4.0	4.421	1.770	0.832	1.522	3.406	0.876	0.224	3.425	0.811	0.221	0.292	2.502
4000/0.50/+0.25	K4.3	4.115	1.683	0.818	1.524	3.433	0.902	0.207	3.452	0.834	0.204	0.264	2.509
4000/1.00/+0.25	K4.5	3.783	1.599	0.810	1.533	3.463	0.921	0.193	3.481	0.851	0.188	0.235	2.513
4000/1.50/+0.25	K4.9	3.452	1.518	0.806	1.547	3.492	0.936	0.182	3.509	0.864	0.177	0.206	2.514
3900/-0.50/+0.25	K4.3	4.793	1.908	0.900	1.636	3.605	0.903	0.264	3.625	0.835	0.261	0.329	2.565
3900/0.00/+0.25	K4.7	4.520	1.813	0.881	1.639	3.642	0.936	0.243	3.661	0.865	0.239	0.299	2.577
3900/0.50/+0.25	K5.4	4.180	1.713	0.869	1.661	3.693	0.961	0.224	3.711	0.888	0.219	0.270	2.583
3900/1.00/+0.25	M0.0	3.812	1.615	0.862	1.687	3.742	0.980	0.208	3.759	0.905	0.204	0.240	2.586
3900/1.50/+0.25	M0.8	3.440	1.517	0.859	1.716	3.792	0.993	0.197	3.808	0.916	0.191	0.212	2.588
3800/-0.50/+0.25	K5.3	4.837	1.944	0.954	1.775	3.876	0.967	0.284	3.894	0.894	0.281	0.337	2.640
3800/0.00/+0.25	M0.3	4.531	1.834	0.939	1.805	3.945	0.999	0.262	3.963	0.924	0.258	0.306	2.652
3800/0.50/+0.25	M1.5	4.144	1.711	0.931	1.858	4.036	1.024	0.242	4.053	0.945	0.237	0.276	2.658
3800/1.00/+0.25	M2.3	3.724	1.589	0.924	1.906	4.119	1.040	0.225	4.134	0.960	0.219	0.246	2.661
3800/1.50/+0.25	M2.8	3.310	1.470	0.919	1.948	4.191	1.053	0.213	4.204	0.971	0.206	0.216	2.662
3700/-0.50/+0.25	M1.4	4.762	1.946	1.023	1.981	4.236	1.036	0.306	4.253	0.958	0.303	0.346	2.718
3700/0.00/+0.25	M2.6	4.403	1.810	1.012	2.049	4.361	1.068	0.282	4.378	0.986	0.277	0.313	2.730
3700/0.50/+0.25	M3.6	3.958	1.658	1.003	2.130	4.504	1.090	0.261	4.519	1.006	0.254	0.282	2.736
3700/1.00/+0.25	M4.1	3.496	1.514	0.992	2.184	4.614	1.106	0.243	4.627	1.019	0.237	0.251	2.739
3700/1.50/+0.25	M4.4	3.059	1.381	0.978	2.216	4.693	1.117	0.229	4.705	1.029	0.221	0.221	2.740
3600/-0.50/+0.25	M3.6	4.522	1.889	1.106	2.277	4.742	1.111	0.329	4.756	1.027	0.324	0.355	2.798
3600/0.00/+0.25	M4.4	4.114	1.734	1.090	2.362	4.920	1.141	0.303	4.933	1.054	0.298	0.321	2.809
3600/0.50/+0.25	M5.1	3.639	1.567	1.070	2.429	5.088	1.161	0.281	5.100	1.071	0.273	0.289	2.815
3600/1.00/+0.25	M5.5	3.166	1.412	1.045	2.453	5.198	1.177	0.262	5.209	1.084	0.254	0.257	2.818
3600/1.50/+0.25	M5.7	2.737	1.274	1.021	2.450	5.261	1.188	0.247	5.269	1.093	0.238	0.226	2.818
3500/-0.50/+0.25	M5.4	4.126	1.782	1.185	2.613	5.402	1.193	0.352	5.414	1.100	0.347	0.366	2.881
3500/0.00/+0.25	M5.8	3.736	1.638	1.149	2.642	5.573	1.222	0.326	5.584	1.126	0.319	0.330	2.891
3500/0.50/+0.25	>M6	3.285	1.480	1.107	2.644	5.713	1.242	0.302	5.723	1.144	0.294	0.296	2.896
3500/1.00/+0.25	>M6	2.839	1.325	1.067	2.618	5.790	1.257	0.283	5.799	1.156	0.273	0.263	2.899
3500/1.50/+0.25	>M6	2.441	1.184	1.035	2.585	5.817	1.268	0.267	5.824	1.165	0.257	0.232	2.899
3400/-0.50/+0.25	>M6	3.695	1.680	1.212	2.833	6.141	1.286	0.377	6.152	1.184	0.371	0.380	2.964
3400/0.00/+0.25	>M6	3.372	1.564	1.156	2.778	6.247	1.317	0.350	6.256	1.210	0.342	0.342	2.972
3400/0.50/+0.25	>M6	2.992	1.419	1.107	2.723	6.313	1.339	0.326	6.321	1.229	0.316	0.306	2.977
3400/1.00/+0.25	>M6	2.602	1.270	1.072	2.675	6.328	1.355	0.306	6.335	1.242	0.294	0.271	2.979
3400/1.50/+0.25	>M6	2.249	1.134	1.048	2.642	6.306	1.365	0.289	6.311	1.251	0.277	0.239	2.978
3300/-0.50/+0.25	>M6	3.185	1.541	1.121	2.806	7.122	1.416	0.408	7.129	1.297	0.399	0.408	3.046
3300/0.00/+0.25	>M6	2.893	1.406	1.082	2.770	7.132	1.445	0.381	7.137	1.322	0.369	0.366	3.053
3300/0.50/+0.25	>M6	2.568	1.254	1.056	2.750	7.093	1.463	0.355	7.098	1.338	0.343	0.325	3.057
3300/1.00/+0.25	>M6	2.239	1.110	1.042	2.743	7.024	1.475	0.334	7.028	1.349	0.320	0.287	3.059
3300/1.50/+0.25	>M6	1.958	0.991	1.039	2.741	6.928	1.481	0.317	6.930	1.354	0.301	0.252	3.058
3200/-0.50/+0.25	>M6	2.917	1.433	1.137	2.807	7.916	1.582	0.449	7.919	1.444	0.436	0.437	3.125
3200/0.00/+0.25	>M6	2.658	1.307	1.104	2.799	7.820	1.599	0.417	7.823	1.459	0.402	0.388	3.133
3200/0.50/+0.25	>M6	2.379	1.175	1.086	2.802	7.696	1.609	0.390	7.697	1.468	0.373	0.343	3.136
3200/1.00/+0.25	>M6	2.107	1.054	1.080	2.811	7.559	1.612	0.366	7.560	1.473	0.347	0.301	3.138
3200/1.50/+0.25	>M6	1.905	0.973	1.091	2.829	7.396	1.611	0.344	7.396	1.472	0.325	0.264	3.136

TABLE 5. (continued)

$T_{\text{eff}}/\log g/[\text{Fe}/\text{H}]$	Type <sup>a</sup>	Johnson-Cousins				Johnson-Glass			CIT/CTIO				
		U-V	B-V	V-R	V-I	V-K	J-K	H-K	V-K	J-K	H-K	CO <sup>b</sup>	BC <sub>K</sub> <sup>c</sup>
3100/-0.50/+0.25	>M6	2.955	1.489	1.266	2.937	8.382	1.756	0.490	8.382	1.601	0.471	0.454	3.203
3100/0.00/+0.25	>M6	2.710	1.361	1.231	2.924	8.256	1.764	0.455	8.256	1.608	0.436	0.402	3.210
3100/0.50/+0.25	>M6	2.431	1.226	1.203	2.919	8.118	1.765	0.424	8.118	1.610	0.403	0.355	3.215
3100/1.00/+0.25	>M6	2.183	1.114	1.191	2.928	7.961	1.760	0.395	7.960	1.606	0.373	0.313	3.217
3100/1.50/+0.25	>M6	2.051	1.069	1.201	2.954	7.751	1.744	0.369	7.748	1.592	0.346	0.271	3.209
3000/-0.50/+0.25	>M6	3.101	1.603	1.400	3.092	8.764	1.937	0.532	8.763	1.764	0.508	0.470	3.281
3000/0.00/+0.25	>M6	2.868	1.478	1.364	3.075	8.638	1.936	0.493	8.636	1.764	0.468	0.416	3.289
3000/0.50/+0.25	>M6	2.604	1.346	1.334	3.064	8.495	1.928	0.457	8.492	1.757	0.431	0.368	3.292
3000/1.00/+0.25	>M6	2.399	1.253	1.317	3.068	8.309	1.908	0.424	8.306	1.740	0.397	0.321	3.288
3000/1.50/+0.25	>M6	2.325	1.235	1.315	3.082	8.043	1.863	0.402	8.039	1.700	0.375	0.278	3.274
4000/-0.50/0.00	<K4	4.454	1.813	0.848	1.547	3.431	0.871	0.224	3.451	0.807	0.221	0.309	2.488
4000/0.00/0.00	<K4	4.178	1.725	0.822	1.520	3.430	0.901	0.206	3.448	0.833	0.204	0.279	2.496
4000/0.50/0.00	<K4	3.870	1.640	0.804	1.505	3.435	0.922	0.193	3.453	0.853	0.188	0.249	2.501
4000/1.00/0.00	K4.1	3.557	1.561	0.793	1.500	3.447	0.940	0.181	3.464	0.867	0.177	0.220	2.504
4000/1.50/0.00	K4.3	3.254	1.488	0.789	1.505	3.464	0.952	0.173	3.481	0.879	0.167	0.192	2.505
3900/-0.50/0.00	K4.2	4.574	1.869	0.894	1.645	3.645	0.932	0.243	3.665	0.862	0.240	0.318	2.563
3900/0.00/0.00	K4.4	4.296	1.775	0.869	1.626	3.653	0.960	0.224	3.671	0.888	0.220	0.286	2.571
3900/0.50/0.00	K4.7	3.973	1.683	0.853	1.621	3.668	0.982	0.208	3.685	0.907	0.204	0.255	2.575
3900/1.00/0.00	K5.0	3.635	1.597	0.844	1.626	3.690	0.997	0.197	3.706	0.921	0.191	0.226	2.577
3900/1.50/0.00	K5.4	3.301	1.513	0.839	1.641	3.719	1.010	0.187	3.735	0.932	0.181	0.198	2.578
3800/-0.50/0.00	K4.9	4.637	1.914	0.946	1.768	3.897	0.996	0.264	3.914	0.921	0.260	0.325	2.637
3800/0.00/0.00	K5.5	4.352	1.811	0.924	1.766	3.923	1.024	0.244	3.940	0.946	0.239	0.293	2.645
3800/0.50/0.00	M0.2	4.004	1.706	0.910	1.779	3.960	1.044	0.227	3.977	0.964	0.221	0.261	2.650
3800/1.00/0.00	M0.9	3.630	1.603	0.902	1.802	4.003	1.059	0.214	4.018	0.977	0.207	0.231	2.651
3800/1.50/0.00	M1.5	3.258	1.501	0.898	1.834	4.054	1.070	0.203	4.068	0.987	0.197	0.202	2.652
3700/-0.50/0.00	M0.5	4.612	1.936	1.010	1.937	4.212	1.065	0.285	4.228	0.985	0.280	0.332	2.715
3700/0.00/0.00	M1.5	4.301	1.815	0.992	1.966	4.276	1.092	0.264	4.292	1.009	0.259	0.299	2.723
3700/0.50/0.00	M2.3	3.917	1.689	0.980	2.005	4.349	1.111	0.246	4.364	1.025	0.239	0.266	2.727
3700/1.00/0.00	M3.0	3.503	1.564	0.971	2.045	4.422	1.124	0.232	4.435	1.036	0.224	0.235	2.729
3700/1.50/0.00	M3.3	3.098	1.442	0.963	2.082	4.490	1.135	0.220	4.503	1.045	0.212	0.206	2.730
3600/-0.50/0.00	M2.7	4.454	1.911	1.087	2.183	4.637	1.139	0.308	4.653	1.052	0.303	0.339	2.796
3600/0.00/0.00	M3.5	4.100	1.769	1.071	2.242	4.753	1.164	0.286	4.767	1.074	0.279	0.305	2.802
3600/0.50/0.00	M4.2	3.686	1.623	1.055	2.292	4.862	1.181	0.266	4.874	1.089	0.259	0.272	2.806
3600/1.00/0.00	M4.5	3.250	1.481	1.039	2.325	4.948	1.194	0.250	4.960	1.100	0.243	0.240	2.809
3600/1.50/0.00	M4.8	2.836	1.349	1.024	2.346	5.018	1.203	0.238	5.028	1.107	0.230	0.211	2.810
3500/-0.50/0.00	M4.5	4.141	1.827	1.173	2.500	5.208	1.218	0.332	5.221	1.123	0.326	0.348	2.877
3500/0.00/0.00	M5.1	3.771	1.680	1.147	2.547	5.351	1.241	0.308	5.362	1.145	0.300	0.312	2.884
3500/0.50/0.00	M5.5	3.361	1.531	1.118	2.567	5.460	1.258	0.288	5.471	1.158	0.279	0.278	2.889
3500/1.00/0.00	M5.7	2.936	1.387	1.090	2.565	5.533	1.270	0.271	5.543	1.168	0.261	0.246	2.890
3500/1.50/0.00	M5.8	2.543	1.253	1.065	2.550	5.579	1.278	0.258	5.586	1.175	0.247	0.216	2.890
3400/-0.50/0.00	M5.9	3.745	1.714	1.235	2.784	5.887	1.304	0.357	5.897	1.202	0.350	0.358	2.959
3400/0.00/0.00	>M6	3.412	1.593	1.190	2.767	5.996	1.327	0.332	6.006	1.223	0.323	0.321	2.966
3400/0.50/0.00	>M6	3.050	1.458	1.148	2.732	6.063	1.345	0.311	6.072	1.237	0.300	0.285	2.969
3400/1.00/0.00	>M6	2.666	1.315	1.113	2.694	6.099	1.359	0.294	6.105	1.248	0.283	0.252	2.970
3400/1.50/0.00	>M6	2.319	1.189	1.087	2.659	6.099	1.368	0.280	6.104	1.256	0.267	0.221	2.970

TABLE 5. (continued)

$T_{\text{eff}}/\log g/[\text{Fe}/\text{H}]$	Type <sup>a</sup>	Johnson-Cousins				Johnson-Glass			CIT/CTIO				
		U-V	B-V	V-R	V-I	V-K	J-K	H-K	V-K	J-K	H-K	CO <sup>b</sup>	BC <sub>K</sub> <sup>c</sup>
3300/-0.50/0.00	>M6	3.279	1.592	1.214	2.919	6.744	1.410	0.386	6.751	1.295	0.376	0.376	3.042
3300/0.00/0.00	>M6	2.990	1.475	1.165	2.860	6.780	1.436	0.361	6.788	1.318	0.349	0.336	3.049
3300/0.50/0.00	>M6	2.688	1.343	1.133	2.814	6.766	1.453	0.339	6.772	1.333	0.325	0.298	3.051
3300/1.00/0.00	>M6	2.353	1.200	1.110	2.788	6.744	1.466	0.321	6.748	1.344	0.306	0.264	3.052
3300/1.50/0.00	>M6	2.076	1.087	1.099	2.770	6.679	1.474	0.305	6.682	1.350	0.291	0.232	3.052
3200/-0.50/0.00	>M6	2.890	1.456	1.153	2.860	7.653	1.560	0.423	7.657	1.426	0.410	0.404	3.124
3200/0.00/0.00	>M6	2.634	1.335	1.127	2.855	7.586	1.577	0.395	7.589	1.442	0.380	0.359	3.129
3200/0.50/0.00	>M6	2.385	1.213	1.118	2.857	7.483	1.589	0.371	7.485	1.453	0.355	0.317	3.132
3200/1.00/0.00	>M6	2.129	1.096	1.116	2.864	7.370	1.597	0.350	7.371	1.460	0.333	0.279	3.133
3200/1.50/0.00	>M6	1.962	1.033	1.133	2.875	7.209	1.597	0.331	7.211	1.460	0.313	0.244	3.132
3100/-0.50/0.00	>M6	2.871	1.468	1.243	2.933	8.232	1.731	0.465	8.233	1.579	0.446	0.424	3.203
3100/0.00/0.00	>M6	2.628	1.347	1.217	2.937	8.117	1.739	0.433	8.118	1.588	0.413	0.375	3.209
3100/0.50/0.00	>M6	2.386	1.225	1.203	2.946	7.979	1.742	0.405	7.979	1.591	0.384	0.331	3.212
3100/1.00/0.00	>M6	2.174	1.136	1.204	2.966	7.813	1.739	0.380	7.813	1.589	0.358	0.291	3.212
3100/1.50/0.00	>M6	2.100	1.118	1.228	2.993	7.580	1.724	0.357	7.579	1.575	0.336	0.250	3.204
3000/-0.50/0.00	>M6	3.020	1.575	1.375	3.078	8.649	1.910	0.507	8.648	1.742	0.483	0.440	3.282
3000/0.00/0.00	>M6	2.783	1.455	1.346	3.075	8.526	1.910	0.470	8.525	1.743	0.445	0.389	3.288
3000/0.50/0.00	>M6	2.555	1.336	1.326	3.079	8.373	1.903	0.437	8.372	1.737	0.412	0.344	3.290
3000/1.00/0.00	>M6	2.392	1.271	1.322	3.098	8.169	1.882	0.408	8.166	1.718	0.382	0.298	3.283
3000/1.50/0.00	>M6	2.359	1.269	1.326	3.109	7.849	1.820	0.389	7.847	1.663	0.362	0.255	3.259
4000/-0.50/-0.50	<K4	4.034	1.751	0.850	1.585	3.503	0.904	0.186	3.522	0.837	0.184	0.273	2.491
4000/0.00/-0.50	<K4	3.763	1.654	0.811	1.528	3.468	0.930	0.176	3.487	0.860	0.172	0.245	2.493
4000/0.50/-0.50	<K4	3.476	1.566	0.785	1.492	3.449	0.948	0.167	3.466	0.876	0.164	0.216	2.493
4000/1.00/-0.50	<K4	3.187	1.489	0.770	1.473	3.443	0.963	0.162	3.459	0.889	0.158	0.189	2.493
4000/1.50/-0.50	<K4	2.918	1.423	0.764	1.465	3.444	0.974	0.160	3.460	0.899	0.154	0.164	2.493
3900/-0.50/-0.50	<K4	4.168	1.812	0.894	1.669	3.702	0.965	0.205	3.720	0.892	0.201	0.283	2.564
3900/0.00/-0.50	<K4	3.902	1.715	0.856	1.614	3.670	0.990	0.193	3.687	0.915	0.188	0.253	2.566
3900/0.50/-0.50	<K4	3.614	1.627	0.831	1.583	3.651	1.008	0.184	3.669	0.931	0.179	0.223	2.567
3900/1.00/-0.50	K4.0	3.315	1.548	0.818	1.566	3.647	1.022	0.178	3.663	0.943	0.172	0.196	2.566
3900/1.50/-0.50	K4.2	3.031	1.478	0.811	1.562	3.655	1.032	0.175	3.669	0.952	0.168	0.170	2.566
3800/-0.50/-0.50	K4.1	4.271	1.870	0.942	1.766	3.924	1.029	0.225	3.941	0.952	0.220	0.291	2.639
3800/0.00/-0.50	K4.2	4.015	1.775	0.906	1.717	3.895	1.055	0.212	3.911	0.974	0.206	0.260	2.640
3800/0.50/-0.50	K4.4	3.726	1.683	0.883	1.692	3.885	1.072	0.202	3.900	0.989	0.195	0.230	2.640
3800/1.00/-0.50	K4.6	3.414	1.598	0.870	1.685	3.890	1.085	0.195	3.904	1.001	0.188	0.201	2.640
3800/1.50/-0.50	K5.0	3.108	1.518	0.864	1.691	3.907	1.095	0.191	3.920	1.009	0.184	0.175	2.640
3700/-0.50/-0.50	K4.6	4.340	1.924	0.998	1.883	4.177	1.100	0.246	4.193	1.016	0.241	0.298	2.716
3700/0.00/-0.50	K5.0	4.080	1.824	0.964	1.848	4.160	1.123	0.233	4.176	1.036	0.226	0.266	2.717
3700/0.50/-0.50	K5.5	3.782	1.724	0.943	1.839	4.167	1.140	0.221	4.182	1.052	0.214	0.235	2.717
3700/1.00/-0.50	M0.2	3.445	1.622	0.931	1.848	4.194	1.152	0.214	4.207	1.062	0.206	0.206	2.717
3700/1.50/-0.50	M1.0	3.105	1.522	0.926	1.871	4.232	1.161	0.208	4.244	1.069	0.200	0.179	2.717
3600/-0.50/-0.50	M5.8	4.347	1.959	1.062	2.040	4.483	1.174	0.270	4.499	1.084	0.264	0.305	2.794
3600/0.00/-0.50	M0.8	4.060	1.846	1.033	2.032	4.500	1.196	0.255	4.515	1.104	0.247	0.272	2.796
3600/0.50/-0.50	M1.8	3.732	1.723	1.015	2.049	4.542	1.211	0.242	4.555	1.117	0.233	0.240	2.796
3600/1.00/-0.50	M2.4	3.361	1.599	1.005	2.080	4.599	1.222	0.233	4.610	1.126	0.224	0.211	2.796
3600/1.50/-0.50	M3.0	2.993	1.480	0.998	2.112	4.656	1.231	0.226	4.667	1.132	0.217	0.183	2.797

TABLE 5. (continued)

$T_{\text{eff}}/\log g/[\text{Fe}/\text{H}]$	Type <sup>a</sup>	Johnson-Cousins				Johnson-Glass			CIT/CTIO				
		U-V	B-V	V-R	V-I	V-K	J-K	H-K	V-K	J-K	H-K	CO <sup>b</sup>	BC <sub>K</sub> <sup>c</sup>
3500/-0.50/-0.50	M2.1	4.249	1.947	1.142	2.270	4.893	1.253	0.296	4.908	1.156	0.287	0.311	2.875
3500/0.00/-0.50	M3.0	3.907	1.813	1.116	2.294	4.958	1.274	0.278	4.972	1.174	0.269	0.277	2.877
3500/0.50/-0.50	M3.6	3.546	1.670	1.098	2.330	5.037	1.287	0.264	5.048	1.186	0.254	0.245	2.877
3500/1.00/-0.50	M4.1	3.155	1.527	1.082	2.361	5.112	1.297	0.254	5.123	1.194	0.244	0.215	2.878
3500/1.50/-0.50	M4.4	2.783	1.400	1.069	2.380	5.173	1.305	0.246	5.182	1.199	0.236	0.187	2.879
3400/-0.50/-0.50	M4.1	4.014	1.866	1.232	2.579	5.455	1.337	0.322	5.467	1.234	0.312	0.319	2.956
3400/0.00/-0.50	M4.6	3.629	1.725	1.201	2.600	5.545	1.357	0.303	5.555	1.250	0.292	0.283	2.957
3400/0.50/-0.50	M5.0	3.268	1.583	1.173	2.612	5.625	1.369	0.287	5.635	1.260	0.277	0.250	2.959
3400/1.00/-0.50	M5.3	2.896	1.444	1.149	2.612	5.687	1.379	0.276	5.695	1.268	0.264	0.220	2.959
3400/1.50/-0.50	M5.4	2.558	1.322	1.129	2.602	5.718	1.387	0.267	5.724	1.274	0.256	0.192	2.959
3300/-0.50/-0.50	M5.9	3.653	1.732	1.310	2.903	6.193	1.430	0.349	6.202	1.317	0.338	0.329	3.039
3300/0.00/-0.50	M5.9	3.291	1.618	1.262	2.860	6.229	1.448	0.329	6.236	1.332	0.317	0.292	3.040
3300/0.50/-0.50	M5.9	2.976	1.498	1.224	2.821	6.258	1.462	0.313	6.264	1.344	0.300	0.257	3.041
3300/1.00/-0.50	M5.9	2.659	1.376	1.194	2.786	6.268	1.473	0.301	6.274	1.353	0.286	0.226	3.042
3300/1.50/-0.50	M5.9	2.406	1.280	1.177	2.757	6.232	1.480	0.290	6.237	1.358	0.276	0.198	3.041
3200/-0.50/-0.50	>M6	3.178	1.584	1.290	3.052	7.142	1.545	0.382	7.148	1.419	0.367	0.348	3.123
3200/0.00/-0.50	>M6	2.856	1.473	1.253	3.006	7.091	1.563	0.361	7.096	1.434	0.345	0.308	3.124
3200/0.50/-0.50	>M6	2.604	1.362	1.231	2.975	7.034	1.576	0.343	7.037	1.445	0.326	0.271	3.125
3200/1.00/-0.50	>M6	2.393	1.270	1.223	2.948	6.937	1.584	0.327	6.939	1.452	0.310	0.238	3.124
3200/1.50/-0.50	>M6	2.307	1.244	1.232	2.923	6.754	1.583	0.314	6.756	1.451	0.297	0.206	3.118
3100/-0.50/-0.50	>M6	3.026	1.545	1.273	3.031	7.891	1.695	0.421	7.893	1.551	0.403	0.368	3.204
3100/0.00/-0.50	>M6	2.713	1.423	1.259	3.040	7.787	1.707	0.396	7.790	1.562	0.377	0.326	3.207
3100/0.50/-0.50	>M6	2.497	1.322	1.258	3.051	7.654	1.713	0.373	7.655	1.568	0.353	0.287	3.207
3100/1.00/-0.50	>M6	2.369	1.271	1.277	3.066	7.456	1.710	0.353	7.456	1.565	0.333	0.249	3.202
3100/1.50/-0.50	>M6	2.391	1.295	1.302	3.058	7.135	1.669	0.342	7.135	1.528	0.320	0.211	3.178
3000/-0.50/-0.50	>M6	3.136	1.621	1.361	3.106	8.405	1.869	0.461	8.405	1.707	0.438	0.385	3.284
3000/0.00/-0.50	>M6	2.834	1.501	1.348	3.129	8.277	1.870	0.431	8.276	1.710	0.408	0.340	3.286
3000/0.50/-0.50	>M6	2.639	1.415	1.352	3.159	8.092	1.862	0.403	8.090	1.703	0.378	0.297	3.282
3000/1.00/-0.50	>M6	2.563	1.384	1.370	3.183	7.815	1.827	0.385	7.814	1.671	0.360	0.256	3.269
3000/1.50/-0.50	>M6	2.570	1.378	1.357	3.140	7.266	1.647	0.385	7.263	1.505	0.362	0.191	3.170
4000/-0.50/-1.00	<K4	3.866	1.736	0.877	1.654	3.592	0.918	0.159	3.609	0.848	0.155	0.238	2.502
4000/0.00/-1.00	<K4	3.558	1.626	0.820	1.563	3.519	0.943	0.155	3.536	0.871	0.151	0.211	2.499
4000/0.50/-1.00	<K4	3.261	1.526	0.780	1.502	3.473	0.961	0.153	3.489	0.888	0.148	0.184	2.496
4000/1.00/-1.00	<K4	2.972	1.442	0.758	1.466	3.449	0.976	0.153	3.464	0.899	0.148	0.158	2.492
4000/1.50/-1.00	<K4	2.710	1.376	0.747	1.450	3.441	0.986	0.156	3.455	0.908	0.151	0.135	2.488
3900/-0.50/-1.00	<K4	4.022	1.805	0.921	1.737	3.798	0.981	0.176	3.815	0.907	0.172	0.249	2.577
3900/0.00/-1.00	<K4	3.709	1.692	0.864	1.646	3.721	1.005	0.171	3.738	0.928	0.166	0.220	2.573
3900/0.50/-1.00	<K4	3.409	1.593	0.826	1.587	3.675	1.024	0.167	3.690	0.944	0.162	0.192	2.569
3900/1.00/-1.00	<K4	3.118	1.508	0.804	1.552	3.648	1.036	0.169	3.664	0.955	0.162	0.166	2.566
3900/1.50/-1.00	<K4	2.848	1.440	0.793	1.534	3.638	1.046	0.171	3.653	0.963	0.165	0.142	2.563
3800/-0.50/-1.00	K4.0	4.159	1.870	0.970	1.829	4.017	1.048	0.195	4.033	0.968	0.191	0.258	2.650
3800/0.00/-1.00	<K4	3.847	1.760	0.914	1.740	3.942	1.071	0.188	3.958	0.989	0.183	0.228	2.647
3800/0.50/-1.00	<K4	3.549	1.662	0.877	1.682	3.895	1.089	0.185	3.909	1.004	0.179	0.199	2.642
3800/1.00/-1.00	K4.1	3.258	1.576	0.855	1.649	3.870	1.101	0.185	3.883	1.014	0.179	0.172	2.639
3800/1.50/-1.00	K4.2	2.980	1.503	0.844	1.634	3.860	1.110	0.186	3.873	1.021	0.180	0.147	2.636

TABLE 5. (continued)

$T_{\text{eff}}/\log g/[\text{Fe}/\text{H}]$	Type <sup>a</sup>	Johnson-Cousins				Johnson-Glass			CIT/CTIO				
		U-V	B-V	V-R	V-I	V-K	J-K	H-K	V-K	J-K	H-K	CO <sup>b</sup>	BC <sub>K</sub> <sup>c</sup>
3700/-0.50/-1.00	K4.2	4.279	1.940	1.024	1.935	4.260	1.120	0.216	4.275	1.035	0.211	0.266	2.726
3700/0.00/-1.00	K4.2	3.963	1.830	0.970	1.849	4.186	1.143	0.208	4.201	1.054	0.203	0.235	2.723
3700/0.50/-1.00	K4.4	3.668	1.730	0.934	1.797	4.143	1.158	0.204	4.157	1.068	0.197	0.206	2.719
3700/1.00/-1.00	K4.6	3.373	1.638	0.912	1.770	4.122	1.170	0.203	4.136	1.078	0.195	0.178	2.716
3700/1.50/-1.00	K4.9	3.083	1.554	0.901	1.762	4.121	1.177	0.204	4.133	1.083	0.197	0.152	2.713
3600/-0.50/-1.00	K4.7	4.371	2.002	1.085	2.060	4.534	1.197	0.239	4.548	1.105	0.232	0.274	2.803
3600/0.00/-1.00	K4.9	4.048	1.891	1.033	1.985	4.468	1.218	0.230	4.482	1.123	0.223	0.242	2.800
3600/0.50/-1.00	K5.4	3.738	1.782	0.999	1.946	4.438	1.233	0.225	4.450	1.136	0.217	0.212	2.795
3600/1.00/-1.00	M0.0	3.426	1.675	0.979	1.934	4.436	1.242	0.223	4.447	1.144	0.214	0.183	2.792
3600/1.50/-1.00	M0.6	3.117	1.573	0.968	1.941	4.452	1.249	0.223	4.463	1.149	0.213	0.157	2.791
3500/-0.50/-1.00	K5.8	4.418	2.045	1.156	2.223	4.862	1.279	0.265	4.875	1.181	0.257	0.280	2.882
3500/0.00/-1.00	M0.7	4.059	1.920	1.108	2.172	4.824	1.299	0.255	4.836	1.198	0.246	0.247	2.879
3500/0.50/-1.00	M1.6	3.712	1.791	1.077	2.160	4.825	1.313	0.248	4.837	1.208	0.238	0.216	2.876
3500/1.00/-1.00	M2.2	3.371	1.662	1.058	2.169	4.852	1.320	0.244	4.862	1.216	0.234	0.188	2.873
3500/1.50/-1.00	M2.7	3.046	1.546	1.046	2.182	4.879	1.325	0.242	4.888	1.218	0.232	0.161	2.870
3400/-0.50/-1.00	M2.1	4.380	2.037	1.241	2.457	5.294	1.367	0.292	5.307	1.260	0.283	0.286	2.962
3400/0.00/-1.00	M2.9	3.951	1.888	1.197	2.437	5.298	1.386	0.281	5.310	1.277	0.270	0.253	2.959
3400/0.50/-1.00	M3.5	3.562	1.741	1.166	2.442	5.337	1.398	0.272	5.346	1.286	0.261	0.221	2.956
3400/1.00/-1.00	M3.9	3.211	1.604	1.144	2.448	5.370	1.404	0.267	5.378	1.292	0.254	0.192	2.953
3400/1.50/-1.00	M4.0	2.937	1.507	1.127	2.433	5.358	1.408	0.263	5.365	1.294	0.251	0.165	2.949
3300/-0.50/-1.00	M4.3	4.215	1.956	1.335	2.773	5.887	1.461	0.322	5.897	1.346	0.310	0.294	3.043
3300/0.00/-1.00	M4.6	3.741	1.803	1.286	2.740	5.899	1.478	0.308	5.907	1.361	0.296	0.259	3.040
3300/0.50/-1.00	M4.8	3.344	1.664	1.249	2.722	5.927	1.489	0.299	5.934	1.370	0.285	0.227	3.038
3300/1.00/-1.00	M4.9	3.048	1.553	1.222	2.692	5.913	1.495	0.290	5.918	1.374	0.277	0.197	3.034
3300/1.50/-1.00	M4.6	2.900	1.508	1.203	2.638	5.792	1.490	0.286	5.797	1.369	0.272	0.168	3.024
3200/-0.50/-1.00	>M6	3.857	1.810	1.420	3.115	6.732	1.566	0.354	6.739	1.440	0.339	0.306	3.126
3200/0.00/-1.00	>M6	3.411	1.676	1.361	3.040	6.679	1.581	0.339	6.685	1.454	0.323	0.269	3.124
3200/0.50/-1.00	>M6	3.079	1.571	1.322	2.982	6.620	1.592	0.326	6.625	1.462	0.310	0.236	3.122
3200/1.00/-1.00	M5.8	2.921	1.519	1.299	2.915	6.467	1.594	0.315	6.471	1.464	0.299	0.204	3.114
3200/1.50/-1.00	M5.2	2.955	1.539	1.278	2.812	6.133	1.538	0.313	6.137	1.412	0.297	0.167	3.072
3100/-0.50/-1.00	>M6	3.595	1.752	1.419	3.227	7.555	1.694	0.390	7.558	1.554	0.372	0.322	3.208
3100/0.00/-1.00	>M6	3.203	1.618	1.388	3.190	7.431	1.705	0.370	7.433	1.564	0.351	0.284	3.206
3100/0.50/-1.00	>M6	2.962	1.538	1.380	3.161	7.253	1.708	0.352	7.254	1.567	0.333	0.248	3.200
3100/1.00/-1.00	>M6	2.934	1.536	1.377	3.097	6.934	1.684	0.343	6.936	1.544	0.324	0.211	3.181
3100/1.50/-1.00	M5.5	3.037	1.572	1.333	2.937	6.305	1.499	0.360	6.306	1.373	0.342	0.144	3.061
3000/-0.50/-1.00	>M6	3.642	1.806	1.443	3.257	8.141	1.848	0.426	8.143	1.692	0.404	0.337	3.288
3000/0.00/-1.00	>M6	3.302	1.681	1.442	3.280	7.972	1.849	0.400	7.973	1.694	0.378	0.297	3.285
3000/0.50/-1.00	>M6	3.109	1.615	1.453	3.288	7.710	1.829	0.384	7.710	1.676	0.362	0.257	3.272
3000/1.00/-1.00	>M6	3.064	1.593	1.436	3.214	7.171	1.686	0.380	7.171	1.544	0.357	0.199	3.192
3000/1.50/-1.00	M5.9	3.088	1.597	1.386	3.055	6.465	1.444	0.427	6.462	1.319	0.413	0.112	3.034

<sup>a</sup>Spectral type derived from Wing (1971) photometry; see text.

<sup>b</sup>No color calibration applied; see Paper I.

<sup>c</sup>BC<sub>V</sub> = BC<sub>K</sub> - (V-K).

TABLE 6. (Empirical<sup>a</sup> – Model) Optical Color Differences of M Giants

Type	$\Delta V$	$\Delta(B-V)$	$\Delta(V-R)$	$\Delta(V-I)$
M0	-0.003	-0.041	0.003	-0.122
M1	0.144	-0.038	0.021	-0.049
M2	0.075	-0.055	0.016	-0.048
M3	0.096	-0.027	0.019	-0.013
M4	0.166	0.079	0.052	0.023
M5	0.263	0.004	0.140	0.138
M6	0.871	0.113	0.366	0.600
M7	0.990	0.038	0.750	1.227

<sup>a</sup>Empirical colors are measured from the “intrinsic” MK spectra of Fluks et al. (1994).